People's Democratic Republic of Algeria

Ministry of Higher Education and Scientific Research

University Echahid Hamma Lakhdar d'El-Oued

FACULTY OF TECHNOLOGY

DEPARTEMENT OFMECHANIC ENGINEERING

END OF STUDY DISSERTATION

PRESENTED FOR GRADUATION OF

MASTER ACADEMIQUE

Domain : Science and Technology

Field: Mechanical Engineering

Specialty: Energetic mechanics

Theme

Theoretical study of ternary compounds MgSiAs2 and MgGeAs2 using Wien2K code: Photovoltaic application

Presented By:

- **Azzi Charaf Eddine**
- **Youmbai ALMotassim B allah**
- **Settu Taher El Amin**
- **Moume Mohammed**

Dr. Nour din menaser	President
Dr.Mohammed khchana	Examiner
Dr .Seif Din Bousbia	Examiner
Dr. Yousra MEGDOUD	Under supervision:

Academic Year : 2021/2022

Abstract

In this work, we present the results of the structural, electronic, optical properties of MgSiAs2 and MgGeAs2 ternary semiconductors using the FP-LAPW method, based on density functional theory (DFT), in the framework of the GGA approximation. The equilibrium lattice constants and the compressibility modulus for ternary compounds were calculated. The optimized structural equilibrium parameters (a, c) are in good agreement with the available results. Calculations of electronic properties show that ternary compounds are direct bandgap semiconductors.

The dielectric function, the refractive index, the absorption coefficient and the reflectivity of the ternary compounds MgSiAs2 and MgGeAs2 as a function of the energy E in summer perform. the results obtained are in good agreement with other theoretical and experimental work available in the literature.

Keywords :, FP-LAPW, DFT, WC-GGA, mBJ.

الملخص

في هذا العمل ، نقدم نتائج الخصائص التركيبية والإلكترونية والبصرية لأشباه الموصلات الثلاثية MgSiAs2 و MgGeAs2باستخدام طريقة FP-LAPW ، بناءً على نظرية الكثافة الوظيفية (DFT) ، في إطار تقريب GGA.تم حساب ثوابت التوازن الشبكي ومعامل الانضغاط للمركبات الثلاثية. تتوافق معامِلات التوازن البنيوي المُحسَّنة (أ ، ج) جيدًا مع النتائج المتاحة. تظهر حسابات الخصائص الإلكترونية أن المركبات الثلاثية هي أشباه موصلات ذات فجوة نطاق مباشرة.

تؤدي وظيفة العزل الكهربائي ومعامل الانكسار ومعامل الامتصاص وانعكاسية المركبات الثلاثية MgSiAs2 و MgGeAs2كدالة للطاقة E في الصيف. تتوافق النتائج التي تم الحصول عليها بشكل جيد مع الأعمال النظرية والتجريبية الأخرى المتوفرة في الأدبيات.

الكلمات الرئيسية :DFT. FP-LAPW . WC-GGA .mBJ.

DEDICATION

We dedicate our dissertation work to our families and to many friends. A special feeling of gratitude to our loving parents, whose words of encouragement and push for tenacity ring in my ears. Our friends never left our side and they were very special. we will always appreciate all they have done, especially our friend BELGACEM MERGHANI for helping us developing our technology skills, AMAR AMMARI for the many hours of proofreading, and Dr.MEGDOUD YOUSRA for helping us devolpe our skills in the mechanic's lab

APPRECIATION

Above all, praise and gratitude to ALLAH the Almighty for the will, the health, the strength and the patience he has given us for the accomplishment of this .work and the achievement of this objective

This research work was carried out in the laboratory of mecaniques of the Mechanical Engineering Department of Echahid Hamma Lakhder University (El Oued). Our first thanks go to Mr. Director Dr.chamsa ali for welcoming me to his laboratory. My thanks also go to Ms. Megdoud Yousra Doctor at Eloued University. I would like to express my sincere thanks to him for having constantly guided me throughout my project and for the precious advice he gave me and for his helpfulness, .his availability and his constructive advice

I would also like to thank all the people in the laboratory who have .contributed directly or indirectly to the completion of this thesis

Contents

General information on photovoltaic cells

List of Figures

*List of table*s

General introduction

Photovoltaic technology allows the direct transformation of sunlight into electricity. The conversion of light into electricity occurs in semiconductor materials. Photovoltaics can play an important role in the transition to a sustainable energy supply system for the 21st century, and is likely to cover a significant part of the electricity needs of several countries.

The principle of the photovoltaic effect has been known for a long time. Indeed, in 1839, A. Becquerel presented a memoir on the electrical effects produced under the influence of solar rays. He observed that an electric current can be generated by illuminating an electrode that has been immersed in a highly conductive solution. However, this discovery remained unresolved until 1954, the year in which three American researchers designed a photovoltaic cell based on fairly efficient silicon (around 6%) which produced electricity directly from the sun's rays. . Solar energy studies really gained momentum during the oil crisis of the 1970s. Since then, several photovoltaic devices have been developed with varying success. Current technology is shared between monocrystalline silicon (80% of the market) and polycrystalline silicon, whose share is tending to increase. The search for new semiconductors intended for photovoltaic conversion currently focuses on compounds such as chalcopyrite MgGeAs2, and MgSiAs2 .

Semiconductor chalcopyrite compounds of formula II-IV-V2, crystallize in a tetragonal structure with a space group I42d . They possess important and varied properties exploitable in nonlinear optics, solar energy conversion, light emitting diodes and various nonlinear optical devices **[1-4].** These types of materials have fascinating electronic and optical properties as well as a wide band of transparency in the visible and infrared regions **[5].** Among the chalcopyrites II-IV-V2. A large number of compounds belonging to this group have been studied for photovoltaic cell applications.

The work presented in this thesis is organized as follows:

Chapter I: In the first chapter of this thesis, we present the studied materials as well as their general physical properties.

Chapter II: devoted to the formalism of the density functional theory (DFT) where we exposed the basic notions and the various approximations used in this theory.

The calculation method (FP-LAPW) used was detailed in chapter III.

Chapter VI: The fourth chapter summarizes our results, their interpretations as well as a comparison with some theoretical and experimental work available in the literature. Finally, we end our work with a general conclusion.

Chapter I:
General information on photovoltaic cells

I-1. Introduction:

This work is mainly motivated by the study of chalcopyrite semiconductor materials of the Mg-IV-V2 group which have experienced tremendous growth in recent years for the interest of its use in the field of solar cells. In this context.

In this chapter, we use some essential bases in the photovoltaic field. We will thus first approach some notions on the photovoltaic cell and . We will then describe the semiconductors, the cell with physical properties of Mg-IV-V2 ternaries and we end with the applications of photovoltaic energy and their advantages and disadvantages.

The use of solar energy is not only linked to its economic advantages but above all to the protection of the environment or it is necessary to find solutions to the problems of pollution (clean energy). In nature, there are several sources of renewable energy including solar. Solar thermal is technically reliable today and many achievements exist (solar water heaters, solar houses, solar collectors, etc.). In the realization of a thermal solar collector, we try to limit the heat losses as much as possible in order to increase the efficiency.

I-2. The photovoltaic cell:

I-2.1. The history of photovoltaic cells:

The discovery of the photovoltaic effect dates back to the year 1839 when the French physicist A. Becquerel [1] obtained an electric voltage by irradiating a silver electrode in an electrolyte. In 1873, W.Smith [2] demonstrated the existence of the phenomenon of conductivity in selenium. After four years, researchers W.G. Adams and R.E.Day [3] discovered the photovoltaic effect of selenium. In 1914 the conversion efficiency of 1% is reached with the selenium-based cell. Several years later, research led to the development of solar cells and especially their performance. Indeed, in 1954, the first cell based on monocrystalline silicon with a yield of 6% was manufactured at the Bell Telephone laboratory (USA) by D.M. Chapin et al[4]. Subsequently, during the first satellite launches and missions lunar cells, solar cells had a resurgence of interest and they are considered a better solution for the power supply of satellites. in 1958, a cell with an efficiency of 9% was developed and the first satellites powered by solar cells were sent into space. On the other hand, following the economic crisis of the 1970s, the surge in oil prices in 1973 and the accidents at the nuclear installations Three Mile Island (USA 1979), Chernobyl (USSR 1986) and more recently Fukushima (Japan 2011), this which reinforce the general public's interest in renewable energies. In 1973, the University of Delaware installed the first house powered by photovoltaic cells. In 1983, the first car powered by photovoltaic energy traveled a distance of 4000 km in 1995, photovoltaic roof programs connected to the grid were launched in Japan and Germany, and have become widespread since 2001.

I-2.2. Photovoltaic cell:

A photovoltaic cell or solar cell is an electronic component which, exposed to light (photons), generates electricity. It is the photovoltaic effect which is at the origin of the phenomenon. The current obtained is a function of the incident light. The

electricity produced depends on the lighting, the photovoltaic cell produces a direct current thanks to the semiconductor material [5].

I-2.3. The characteristics of the photovoltaic cell:

What is it made of?

To manufacture a photovoltaic cell, we use semiconductor materials, which are electrical insulators, but which still allow electrons to produce current. Silicon is the material most frequently used to manufacture photovoltaic cells.

Silicon has many advantages: it is very abundant and easy to extract (it is found in sand and quartz). It is also easily recyclable. In rare cases, other materials are used to manufacture photovoltaic cells: copper indium gallium selenide, copper-indium selenide, cadmium telluride, or even perovskite. These materials remain very little used for the moment, but a lot of scientific research is interested in them.

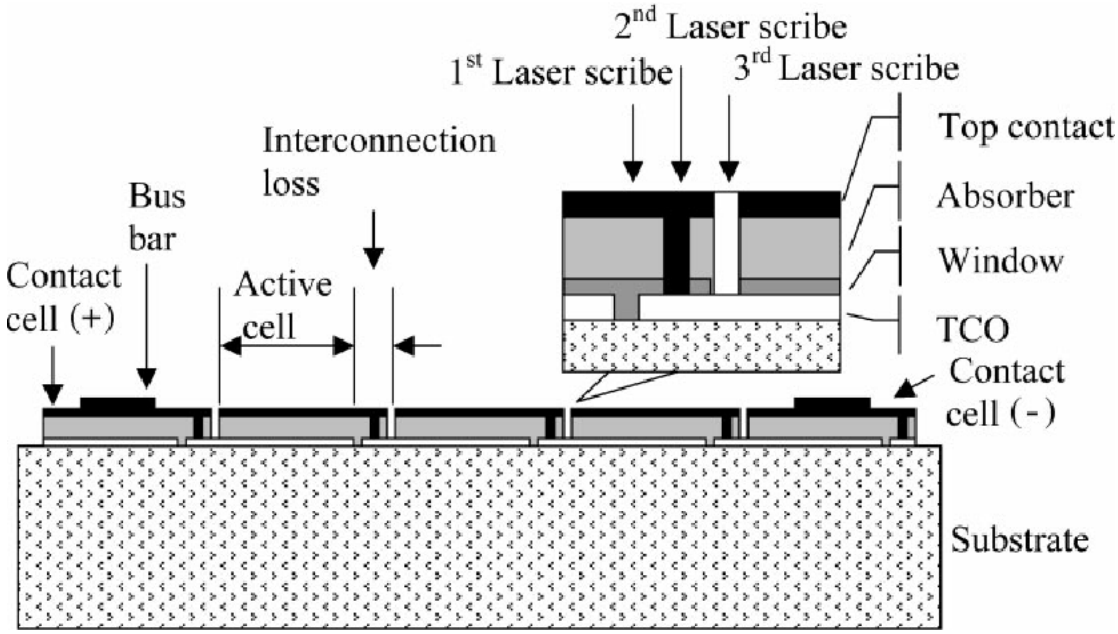

Figure I-1: Simplified diagrams represent the structure of a thin film solar cell.

I-3. Properties of photovoltaic cell components:

I-3.1. The substrate:

The substrate is the support allowing the mechanical strength of the different layers, the stacking of which does not exceed a few micrometers in thickness. The substrate can be made of ordinary or soda glass, it is also possible to use flexible (Duplex type) or metallic substrates. The choice of glass as the deposition substrate was adopted because of the good thermal expansion so as to minimize the stresses at the substrate

layer interface, and for economic reasons, for their transparency which adapts well for the optical characterization of layers in the visible.

I-3.2. Lower ohmic contact:

It is a metallic layer, several materials used, but the most often used is molybdenum (Mo) which is chosen as the best lower ohmic contact [6,7]. because of:

- The low resistance.
- Stability.
- Good adhesion with absorbent layers.

Molybdenum is a metallic gray colored transition metal with a centered cubic crystal structure. It is deposited by sputtering on the glass. the two deposition methods commonly used are deposition by RF radiofrequency [8] and by magnetron [9] under an argon atmosphere. The thickness of the layer varies from 0.3 to 1µm.

I-3.3. The absorption layer:

The absorber is the part of the cell in which the photons will be converted into electron-hole pairs. It is made of a semiconductor material with the following properties:

- High absorption coefficient of the order of $10^4 cm^{-1}$ in the visible range [0.4µm-0.8 µm].
- Length of the direct preference band gap included in the interval [1eV-1.7eV].
- Conductivity must be of the order of 10^{-2}cm (Ωcm^{-1}).
- The type of p-type semiconductor material.

The necessary thickness of the absorbing layer is in the range 1-2µm to absorb all the solar radiation.

I-3.4. Buffer layer (CdS):

It is a layer of an n-type semiconductor material, it consists of cadmium sulphide (CdS) deposited by chemical bath (CBD). It is characterized by:

- A gap of 2.4 eV.
- A conductivity of the order of 10^{-3} $(\Omega cm)^{-1}$ of type n lower than the absorbent layer.
- A strong homogeneous morphology.
- An electron affinity of the same order as that of the absorbent layer.
- A crystalline parameter close to that of the absorbent layer.

I-3.5. The conductive transparent oxide layer (OTC):

The layer is made of a transparent material with a conductivity greater than 10^3 $(\Omega cm)^{-1}$, there is a layer of zinc oxide (i-ZnO, Eg= 3.3 eV) this layer would be used to reduce possible leakage currents at the level of the junction and to protect the interface before the deposition of the conductive transparent oxide layer (Zinc oxide doped with aluminum ZnO:Al, Eg=4eV). must have maximum transparency in order to allow optimal transmission of the incident light useful to the absorber, hence their name window layer.

I-3.6.The upper ohmic contact (metal grid):

Generally it is a layer of about 50 nm of Ni followed by a layer of Al of about 2 to 3 µm and sometimes an antireflection layer (MgF2) is added [10]. The operation of anti-reflective layers is based on the adaptation of the refractive index of the layer so as to produce destructive interference at a certain wavelength taking into account the thickness of the layer. The material used as the anti-reflective layer should be non-absorbent in the solar spectrum range.

I-4.The different photovoltaic cell technologies:

There are a large number of technologies implementing the photovoltaic effect, many are still in the research and development phase [11].

The main technologies industrialized in quantity to date are: mono or polycrystalline silicon (more than 80% of world production) and thin film silicon based on amorphous silicon or CIS (Copper Indium Selenium).

I-4.1. First generation: crystalline silicon:

Solar cells based on crystalline silicon are manufactured from ingots in the form of thin slices by respecting the following steps:

- Extraction of silicon ore.
- Purification of silicon by refining to increase purity.
- In heats the silicon up to melting temperature giving ingots.
- Solidification of material after cooling.
- Surface purification treatment by chemical-physical process.
- Obtaining a fine cell with the electrodes.

The Solar cells are divided into two categories mono or polycrystalline depending on the structure.

I-4.2. Monocrystalline solar cell:

The monocrystalline cell consisting mainly of silicon crystals, composed of a single crystal divided into two layers. This type of cell makes it possible to obtain a very high yield of 18% [12] in the laboratory, despite this it has a very high manufacturing cost because of the very long purification process.

I-4.3. Polycrystalline solar cell:

The polycrystalline cell composed of an aggregate of crystals. It also comes from the sawing of blocks of crystals. This type of cell has a lower efficiency than monocrystalline cells, of the order of 10 to 15% [13] with low production cost and requires less energy.

I-4.3.1. Second generation: amorphous silicon, CdTe and CIS/CIGS:

This generation of cells is based on semiconductor materials in thin layers which can be deposited on the substrate by physical or chemical processes.The thickness of the layer is of the order of a nanometer to a few ten micrometers. There are three sectors for the production of thin-film photovoltaic cells:

- The amorphous silicon sector (α-Si).
- The cadmium telluride (CdTe) and cadmium sulphide (CdS) sector.
- The chain of chalcogenide compounds with a chalcopyrite structure based on CuInSe2.

I-4.3.2. The amorphous silicon (α-Si) sector:

The amorphous silicon-based solar cells are deposited directly on the glass substrates produced in a secondary vacuum chamber. The layers are also obtained by plasma with a high gap compared to the crystalline silicon gap. The absorption coefficient in visible light is 50 times higher than in crystalline silicon with a yield of 10% [14].

I-4.3.3. The chalcopyrite sector based on II-IV-V2:

Ternary semiconductors of Chalcopyrite type (II-IV-V2) crystallize in the tetragonal (quadratic) crystal system a=b≠c and α=β=γ=90, with space group ($I\bar{4}2d$). They consist of three elements: a transition metal (Cu, Ga.,) and a third column element such as (In ...), and a chalcogen, (Se ...). Generally chalcopyrites (II-IV-V2) are composed of a mixture between two Zinc-Blende (GaP) sphalerite structures, type III-V Figure (II.2) binary compounds, introduces a change of symmetry group from ($F\bar{4}3m$) to ($I\bar{4}2d$) thus characterizing a chalcopyrite quadratic structure for these types of crystals. By doubling its unit cube along the z axis which becomes the c axis of the chalcopyrite structure. In the most real chalcopyrite crystals, the c/a ratio is approximately equal to 2. For an ideal chalcopyrite structure c=2a. [15][16].

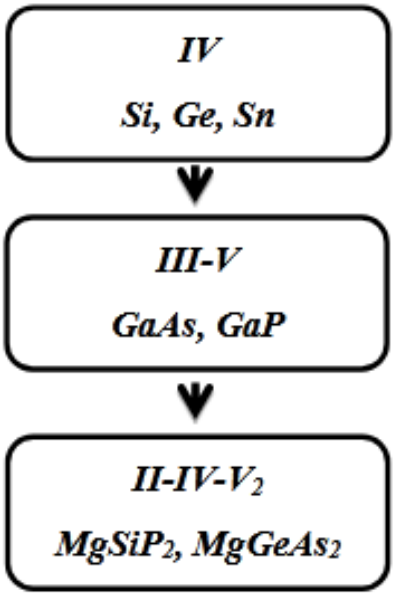

Figure I-2: Origin of a chalcopyrite structure

I-5.Type II-IV-V2 chalcopyrite's:

Recently, much attention has been paid to the study of the optical properties of ternary compounds of chalcopyrite, and are still the subject of much work. They constitute a natural extension of the compounds of structure Zinc-blende (GaP) (III-V) presented in Figure (II (b)). Chalcopyrite presented in Figure (II (a)) is distinguished from sphalerite by an extension along the "c" axis which gives it a quadratic structure.

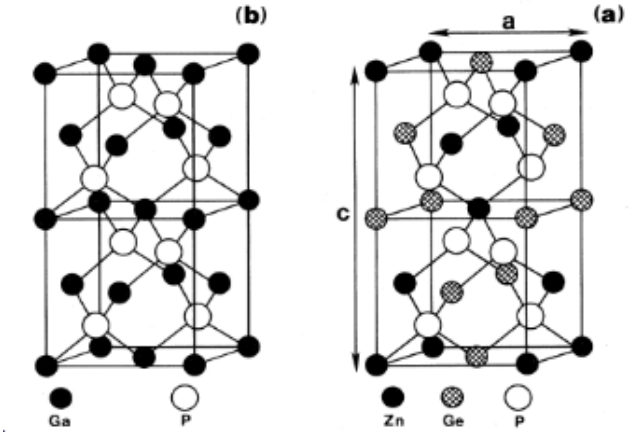

Figure I-3: Comparison of the crystalline structure of a binary zinc-blende (GaP) semiconductor (double cells) with a chalcopyrite (ZnGeP2) structure. [17]

I-5.1. Crystalline structure of some type II-IV-V2 chalcopyrite's:

In the table (I), we present some values of the mesh parameters of the

chalcopyrites:

Table (I): lattice parameters of chalcopyrites

Compound	a=b(*A*°)	c(*A*°)	c/a	u	Référence
$MgSiP_2$	5.700	9.408	1.650	0.288	[6]
$MgSiSb_2$	GGA5.954 LDA5.885	10.800 10.569	1.814 1.796	0.286 0.285	[6]
$MgSiAs_2$	GGA5.733 LDA5.694	10.242 10.124	1.786 1.778	0.292 0.292	[6]
$BeSiP_2$	5.100	10.173	1.994	0.234	[7]
$BeGeAs_2$	5.370	10.873	2.025	0.2177	[7]
BeSnP	5.380	10.816	2.010	0.1935	[7]

In the table (II), we present the coordinates of the different atoms (II, IV, V) in the unit cell of type (II-IV-V2) with chalcopyrite structure.

Table (II): Positions of the atoms of (II, IV, V) in the chalcopyrite lattice of (II-IV-V2).

II	**(0, 0, 0)**	**(0, 1/2, 1/4)**
IV	(1/2, 1/2, 0) (0, 0, 1/2)	(1/2, 0, 1/4) (0,1/2,3/4
V_2	(u, 1/4, 1/8) (-1/4, u, -1/8)	(u, -1/4, 1/8) (1/4, -u, -1/8)

With (u) the displacement of the anion from its ideal position in a chalcopyrite structure is written under the form :

$$\mathbf{u = {}^{1}/_{4} + (\alpha + a^2)} \qquad \textbf{(I)}$$

α: is the deviation of bond lengths.

I-5.2. Physical properties of chalcopyrite materials:

I-5.2.1. Electronic properties:

A useful starting point for a description of the electronic properties of compounds that crystallize in the chalcopyrite phase is the band structure of zinc blende.

The Brillouin zone of the zinc blende is represented with the smaller Brillouin zone of the ternary figure (IV)

The tetragonal symmetry of the chalcopyrite lattice leads to a change in the band structure even in the center of the Brillouin zone (**Γ**) compared to the band structure of the zinc blende. The non-degenerate energy bands at (**Γ**1....4) are formed according to:[17]

$$E(K) = E(\Gamma) + \left(h^2/_2\right)\left(\frac{K_Z^2}{m_{\parallel}} + \frac{\left(k_y^2 + K_X^2\right)}{m_{\perp}}\right) \qquad \textbf{(II)}$$

A function E(k) gives the energies of a band state at a wave vector k in the Brillouin zone. Where k_x, k_y, k_z are the components of the wave vector in an orthogonal frame of reference with axis z parallel to axis c.

$\boldsymbol{m}\parallel$ and $\boldsymbol{m}\perp$. The longitudinal and transverse effective masses Electrons are thus characterized by the two effective masses: $\boldsymbol{m}\parallel$ and $\boldsymbol{m}\perp$. From these two effective masses we define an effective mass density of states:

$m_{ds}^3 = m_{\perp}^2 m_{\parallel}$ **(III)**

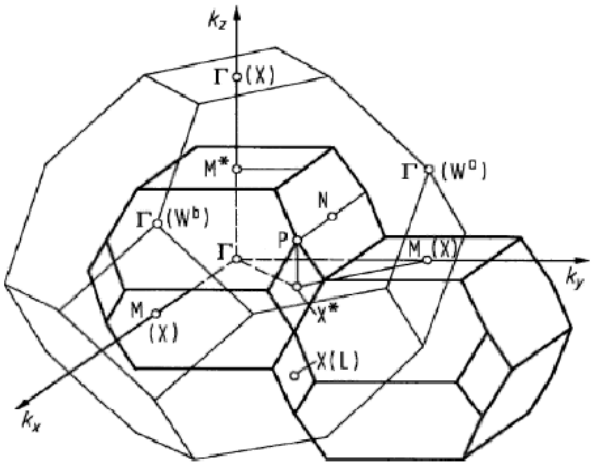

Figure I-4: Two Brillouin zones of zinc blende (thin lines), chalcopyrite (thick lines) [18] M*,X* the points of symmetry of M and X sometimes indicated T(or Z) and N, respectively, in the figures.

It is recalled that the electronic configurations of magnesium, silicon, tin, arsenic, antimony and germanium are as follows:

$_{12}$Mg = [Ne] $3s^2$
$_{14}$Si = [Ne] $3s^2\ 3p^2$
$_{50}$Sn = [Kr] $5s^2\ 5p^2\ 4d^{10}$
$_{33}$As = [Ar] $4s^2\ 4p^3\ 3d^{10}$
$_{51}$Sb = [Kr] $5s^2\ 5p^3\ 4d^{10}$
$_{32}$Ge = [Ar] $4s^2\ 4p^2\ 3d^{10}$

I-5.2.2. First area of Brillouin:

In solid-state physics, the notion of the Brillouin zone is necessary to describe the physical properties of a crystal in which translational symmetry plays a very important role [19].

Solid-state physics theory [20] makes it possible to specify the distribution of energy levels and the primitive Weigner Seitz cell which represents the first Brillouin zone, i.e. the smallest possible volume of the reciprocal lattice.

For the zinc blende type structure, the first Brillouin zone has the shape of an octahedron truncated by the six faces of a cube (figure I.6), and it presents a center of symmetry at the origin noted: Γ . The axes or the lines of high symmetry are: Δ,Λ,Σ, The crossing points of each of these axes with the borders of the first Brillouin zone are the points of high symmetry and they play a major role in the theory band [21].

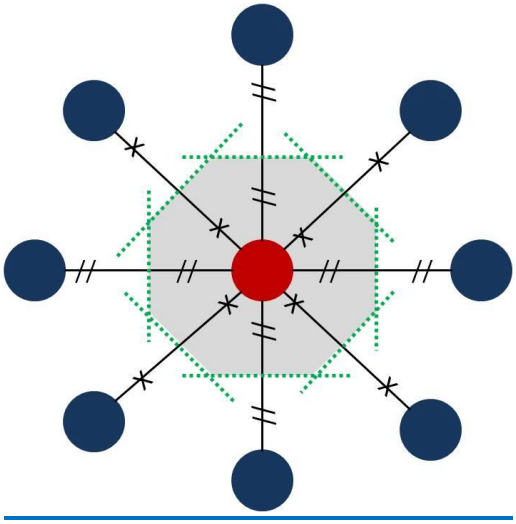

Figure I-5: Two-dimensional Wigner-Seitz construction.

I-6. Characteristics of the Brillouin area:

I-6.1. Points of high symmetry:

Γ: This point is the center of the first Brillouin zone with coordinates K_f=(0.0.0).

X: This point is the center of a square face of the octahedron which belongs to one of the axes Kx, Ky, Kz with one of the square faces. So we have :

$$\mathbf{K_x}= \frac{2\pi}{a} (\pm \mathbf{1}.\mathbf{0}.\mathbf{0})$$

$$\mathbf{K_y}= \frac{2\pi}{a} (\mathbf{0}.\pm \mathbf{1}.\mathbf{0})$$

$$\mathbf{K_z}= \frac{2\pi}{a} (\mathbf{0}.\mathbf{0}.\pm \mathbf{1})$$

L: This point is the center of a hexagonal face of the octahedron whose coordinates are:

$K_l= \frac{2\pi}{a}$ (1.1.1).

W: This point is on one of the vertices of the square faces.

The contact details are:

$K_w = \frac{2\pi}{a}\ (0.\frac{1}{2}.1).$

Z: This point is located on the line which joins the center of a square face to one of the corners of the octahedron with the coordinates:

$K_z = \frac{2\pi}{a}\ (1.\frac{1}{2}.1).$

I-4-1-1-B Lines of high symmetry:

Δ: This line represents the <100> direction. It connects the center Γ to the point X.

Σ: It is a point belonging to the plane of symmetry Kx=Ky or Ky=Kz or Kx=kz.

Λ: This line is the <100> direction. It connects the center of the zone Γ to the center of a hexagonal face which is the point L of the octahedron. (Figure I.7) .

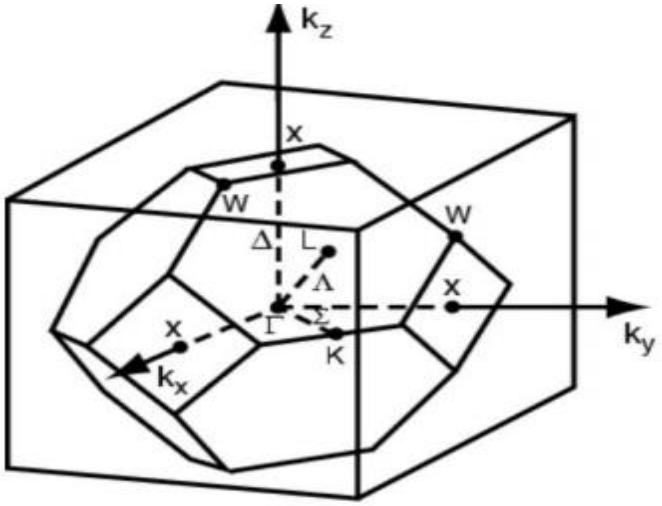

Figure I-6: Brillouin zone of the Zinc blende structure

I-6.2. The band structure of type II-IV-V2 chalcopyrite's:

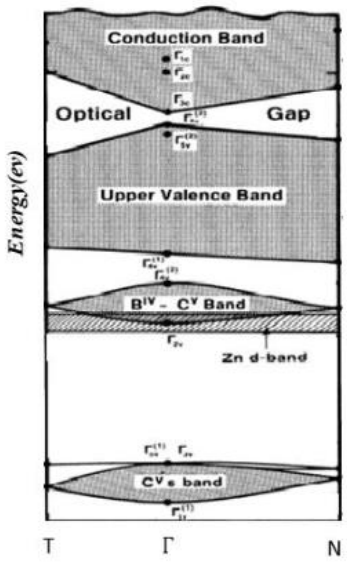

Figure I-6: Energy band structure of II-IV-V2, with indication atomic orbital contributions. [17]

I-6.3. Optical properties:

The different ways in which light interacts with matter are absorption, transmission, reflection, refractive index, scattering or emission. These properties depend on energy. The study of optical properties of solids is a powerful tool to understand the electronic properties of materials because the energy dependence of optical properties is related to the band structure. Therefore, information about the energy eigenvalues and the energy eigenfunction are needed to calculate the frequency-dependent and energy-dependent optical properties. The optical property of some type II-IV-V2 chalcopyrite materials are compared in the table:

Table (III): Characteristics of some ternary chalcopyrites observed at room temperature.

Compound	η=c/2a	E_g (eV)	$n_{a\perp b\parallel}$	$R_{a\perp b\parallel}$	Références
$MgSiP_2$	0.860	$_{BJ}$2.00	$_a$2.826-$_b$2.952	$_a$0.228-$_b$0.244	[6][9]
$MgSiSb_2$	$_{GGA}$0.907 $_{LDA}$0.898	$_{GGA}$0.826 $_{LDA}$0.823	$_a$3.783-$_b$3.836 $_a$3.849-$_b$3.930	$_a$0.339-$_b$0.344 $_a$0.345-$_b$0.353	[6] [7]
MgSiAs2	$_{GGA}$0.893 $_{LDA}$0.889	$_{GGA}$1.20 $_{mBJ}$1.80	$_a$3.386-$_b$3.414 $_a$3.373-$_b$3.419	$_a$0.296-$_b$0.299 $_a$0.295-$_b$0.300	[6] [9]
$BeSiP_2$	0.997	$_{mBJ}$1.74	$_a$4.464-$_b$4.506	$_a$0.574-$_b$0.588	[7]
$BeGeAs_2$	1.006	$_{mBJ}$1.12	$_a$4.129-$_b$4.204	$_a$0.545-$_b$0.555	[7]
$BeSnP_2$	1.005	$_{mBJ}$1.51	$_a$4.130-$_b$4.300	$_a$0.559-$_b$0.564	[7]

With: $\boldsymbol{\eta}$ the distortion ratio.

$n_{a\perp b\parallel}$ The index of refraction

$R_{a\perp b\parallel}$ Reflection

I-7.Advantages and disadvantages of photovoltaic technology

I-7.1. Advantages:

Photovoltaic technology has a number of advantages.

- ✓ Source of energy: inexhaustible, free. So reduction in the energy bill.
- ✓ High reliability: the modules are guaranteed for 25 years by most manufacturers.
- ✓ It has no moving parts, which makes it particularly suitable for remote areas. This is the reason for its use on spacecraft.
- ✓ Their operating costs are very low given the reduced maintenance and they do not require fuel, transport or highly specialized personnel.
- ✓ It is a source of electrical energy without the release of polluting gases or waste and completely silent, which is not the case, for example, with wind turbines. It does not cause any disturbance of the environment.

I-7.2. Disadvantages:

However, the photovoltaic system has drawbacks.

- ✓ The manufacture of the photovoltaic module is high technology and requires high cost investments.
- ✓ The actual conversion efficiency of a module is low (the theoretical limit for a crystalline silicon cell is 28%).
- ✓ Photovoltaic generators are only competitive with diesel generators for low energy demands in isolated regions.
- ✓ Occupation of space for large installations.
- ✓ Finally, when the storage of electrical energy in chemical form (battery) is necessary, the cost of the photovoltaic generator is increased. However, the reliability and performance of the system remain equivalent provided that the battery and the associated regulation components are judiciously chosen.

I-8. Conclusion:

Chalcopyrite's are promising materials in several fields and applications, especially useful for applications in photonics, optoelectronics and optics. In this chapter we have discussed some generalities concerning chalcopyrite materials, their crystalline structures, as well as their uses in the fields of current interest.

Chapter II: Density Functional Theory (DFT)

II-1. INTRODUCTION:

The quantum theory of solids is a branch of physics that studies solids' physical characteristics from their microscopic elements. It's all about characterizing or predicting a solid's characteristics based on its tiny structure and interactions between basic particles, such as the ions and electrons which make it up.

This quantum description of a molecular or crystalline system is based on Schrödinger's equation. The Schrödinger equation is particularly difficult to solve because the electrons and nuclei that make up materials form a strongly interacting many-body system. Because it is difficult to tackle this problem precisely, approximations must be made.

II-2. Equation of SCHRÖDINGER:

The Schrödinger equation of a crystalline system made up of a collection of particles (nuclei plus electrons), is written in the form:

$$\boldsymbol{H\Psi = E\Psi} \qquad \textbf{(II-1)}$$

where

H: represents the Hamiltonian of the crystal system.

Ψ: its system wave function.

E: total system energy.

The Hamiltonian H contains different forms of energy:

$$\boldsymbol{H = T_e + T_n + V_{n-e} + V_{e-e} + V_{n-n}} \qquad \textbf{(II-2)}$$

Te and Tn are, respectively, the kinetic energy of the electron and the nucleus. **Vn-e** is the potential energy of nucleus-electron attraction, while **Ve-e** and **Vn-n** are respectively the potential energy of repulsion between electrons-electrons and nucleus-nucleus:

$\boldsymbol{T_n = -\frac{1}{2}\sum_i \frac{\nabla_i^2}{M_A}}$: The kinetic energy of nuclei.

$\boldsymbol{V_{n-e} = -\sum_i \sum_A \frac{Z_A}{R_{Ai}}}$: The potential energy of nucleus-electron attraction

$\boldsymbol{V_{e-e} = \sum_{i<j} \frac{1}{r_{ij}}}$: The potential energy of repulsion between electrons.

$\boldsymbol{V_{n-n} = \sum_{A<B} \frac{Z_A Z_B}{R_{AB}}}$: The potential energy of interaction between the nuclei.

i and **j** index the electrons, **A** and **B** index the nuclei, $\mathbf{M_A}$ and $\mathbf{Z_A}$ are respectively the mass and the charge of the considered nucleus, $\mathbf{R_{Ai}}$, $\mathbf{r_{ij}}$ and $\mathbf{R_{AB}}$ are respectively the nucleus/electron, electron/electron and nucleus/nucleus distances.

Thus the Hamiltonian **H** can be written, explicitly, as follows:

The potential energy of interaction between nuclei.

i and **j** index the electrons, **A** and **B** index the nuclei, $\mathbf{M_A}$ and $\mathbf{Z_A}$ are respectively the mass and the charge of the considered nucleus, $\mathbf{R_{Ai}}$, $\mathbf{r_{ij}}$ and $\mathbf{R_{AB}}$ are respectively the nucleus/electron, electron/electron and nucleus/nucleus distances.

Thus the Hamiltonian **H** can be written, explicitly, as follows:

$$\boldsymbol{H = -\frac{1}{2}\sum_i \nabla_i^2 - \frac{1}{2}\sum_A \frac{\nabla_i^2}{M_A} - \sum_i \sum_A \frac{Z_A}{R_{Ai}} + \sum_{i<j} \frac{1}{r_{ij}} + \sum_{A<B} \frac{Z_A Z_B}{R_{AB}}} \quad \textbf{(II-3)}$$

The Hamiltonian operator can therefore be decomposed into two contributions, kinetic and potential.

The solution of the Schrödinger equation (II-3) leads to the resolution of a many-body problem. It is out of the question to solve this problem exactly. In order to find approximate acceptable eigenstates, we need to make approximations.

II-3. Fundamental approximations:

II-3-1. BORN-Oppenheimer approximation:

All methods for solving the Schrödinger equation are based on the Born-Oppenheimer approximation [21,22] which is also called the adiabatic approximation. The basic idea is to make the separation between the nuclei and the electrons: As the nuclei are heavier than the electrons, their movement is much slower so we can separate in the expression of

the wave function the electronic contributions and nuclear. The movement of the nuclei is treated classically and that of the electrons in a quantum way.

In this hypothesis, the Schrödinger equation is simplified, taking into account the fact that the kinetic energy Tn becomes zero and the nucleus-nucleus potential energy Vn-n takes a constant value which is considered as a reference. Thus, the Hamiltonian can be put in the following form :

$$\boldsymbol{H = T_e + V_{n-e} + V_{e-e}} \qquad \textbf{(II-4)}$$

and :

$$H = \underbrace{-\frac{1}{2}\sum_i \nabla_i^2}_{T_e} + \underbrace{-\sum_i \sum_A \frac{Z_A}{R_{Ai}}}_{V_{ne}} + \underbrace{\sum_{i<j} \frac{1}{r_{ij}}}_{V_{ee}} \qquad \textbf{(II-5)}$$

However, this approximation is not sufficient on its own to solve Schrödinger's equation, due to the complexity of electron-electron interactions.

II-3-2. The Hartree and Hartree-Fock approximations:

One of the first attempts to solve the Schrödinger equation is proposed by Hartree [21]. This approximation consists in finding the eigenfunctions of H in an approximate form:

$$\boldsymbol{\Psi = \Psi_1(r_1).\Psi_2(r_2).\Psi_3(r_3) \ldots\ldots\ldots \Psi_N(r_N)} \qquad \textbf{(II-6)}$$

The Hartree approximation is based on the assumption of free electrons, which amounts to not taking into account the interactions between electrons and spin states. This has two important consequences:

- The total Coulomb repulsion **Ve-e** of the electronic system is overestimated.
- The Pauli exclusion principle is not taken into account.

This second consequence being more serious than the first, the electronic system in the Hartree approximation is not completely described. The "Hartree-Fock" approximation [22] was introduced to take into account the spin of the electrons in the resolution of the Schrödinger equation.

In 1930, Fock [23] showed that the Hartree wave function (II-6) violates the Pauli exclusion principle because it is not antisymmetric with respect to the exchange of any two particles. The wave function ψ(r1,r2,…rN) is then replaced by a Slater determinant composed of single-electron spin orbitals which respects the antisymmetry of the wave function:

$$\Psi^{HF}(x_1, x_2, x_3, \ldots\ldots, x_N) = \frac{1}{\sqrt{N!}} \begin{vmatrix} \varphi_1(x_1) & .. & \varphi_N(x_1) \\ . & .. & . \\ \varphi_1(x_N) & .. & \varphi_N(x_N) \end{vmatrix} \quad \textbf{(II-7)}$$

Or $\frac{1}{\sqrt{N!}}$ is the normalization factor.

II-3-3. Thomas-Fermi approximation:

The Thomas-Fermi method relies on a statistical model to approximate the electronic distribution around an atom. The mathematical basis used was to postulate that the electrons are uniformly distributed in phase space and that this electron system is subject to a coulomb field which is created by all the fixed nuclei. They were thus able to deduce the kinetic energy of this homogeneous gas of electrons according to its electron density ρ(r) [24, 25, 26].

$$E_c = 3(3\pi^2)^{\frac{2}{3}}\hbar^2\rho^{\frac{3}{5}}/10m \qquad \textbf{(II-8)}$$

Although this is an important first step, the precision of the Thomas-Fermi equation remains however limited, because the functional of the resulting kinetic energy is approximated but also because this method does not take into account the energy of exchange of electrons, a consequence of Pauli's principle, nor of electronic correlation. An energy exchange functional was added by Paul Diracen 1930 [27].

However, the Thomas-Fermi-Dirac method remains relatively imprecise for most applications, the greatest source of error coming from the writing of the kinetic energy which can however be improved by adding to it the correction proposed in 1935 by Carl

von Weizsäcker (1912-2007) who takes into account the density gradient in the expression of the kinetic energy functional: [28].

Density functional theory (DFT) is a very powerful method of simulation and is used as a mathematical tool for solving many-body problems. The objective of DFT methods is to find a functional (i.e. a function dependent on a function) allowing to relate the density with the energy.

DFT has its origins in the model developed by Thomas and Fermi in the late 1920s[29]. Nevertheless, it was not until the mid-1960s and the contributions of Hohenberg, Kohn and Sham [30] that the theoretical formalism on which the current method is based was established. This formalism consists in writing the total energy of the system of electrons in interactions as being a functional of the electron density.

II-4-1.Hohenberg-Kohn theorem:

The foundations of the formalism of density functional theory (DFT) are based on two essential theorems which were stated and proved by Hohenberg and Kohn [31].

Theorem 1:

The first theorem establishes the one-to-one correspondence between the ground state electron density ρ(r) and the external potential Vext. As a consequence, the total energy of the ground-state system is also a universal unique functional of the electron density, such that:

$$E = E[\rho(r)] \qquad \textbf{(II-9)}$$

This theorem means that it suffices to know only the electron density to determine all the wave functions. This is the fundamental result of the theory of density functional (DFT).

Theorem 2:

Hohenberg and Kohn show that the minimum value of this functional is the exact energy of the ground state, and that the density which leads to this energy is the exact density of the ground state. The other properties of the ground state are also functional of this density:

Or :

$$\boldsymbol{E(\rho_0) = minE(\rho)} \qquad \textbf{(II-10)}$$

This theorem means that it is enough to know only the electron density to determine all the wave functions. This is the fundamental result of density functional theory (DFT).

ρ_0: the ground state density.

The functional of the total energy of the ground state is written as follows:

$$\boldsymbol{E[\rho(\vec{r})] = F[\rho(\vec{r})] + \int V_{ext}(\vec{r})\rho(\vec{r})d^3\vec{r}} \qquad \textbf{(II-11)}$$

Or

$$\mathbf{F[\rho(\vec{r})] = \langle \Psi | T + V | \Psi \rangle} \qquad \textbf{(II-12)}$$

Note that the functional F[ρ] is universal for any multi-electron system. If the functional F[ρ] is known, then it will be relatively easy to use the vibrational principle to determine the total energy and ground state electron density for a given external potential. Unfortunately, Hohenberg and Kohn's theorem gives no indication of the form of F[ρ].

Note that the functional F[ρ] is universal for any multi-electron system. If the functional F[ρ] is known, then it will be relatively easy to use the vibrational principle to determine the total energy and ground state electron density for a given external potential. Unfortunately, Hohenberg and Kohn's theorem gives no indication of the form of F[ρ].

II-4-2. Kohn and Sham equations:

The idea of Walter Kohn and Lu Sham [32] in 1965 is to reduce the system of interacting Ne electrons to a fictitious system of independent Ne electrons with the same electron density. The interest comes from the fact that the expressions of the kinetic energy and the potential energy for this fictitious system are known. We thus go from a problem with a wave function ψ(r) with Ne electrons to a problem with Ne mono-electron wave functions Φ(r) called Kohn Sham states. We note Tind[ρ] the kinetic energy of the system of Ne independent electrons and Vind[ρ] the classical potential energy which is the Hartree term*:*

$$\boldsymbol{V_{ind}[\rho] = \frac{1}{2}\int \frac{\rho(r)\rho(r')}{|r-r'|} drdr'} \qquad \textbf{(II-13)}$$

The energy of the system therefore becomes:

$$\boldsymbol{E[\rho] = T_{ind}[\rho] + V_{ind}[\rho] + E_{XC}[\rho] + \int V_{e-n}(r)\rho(r)dr} \quad \textbf{(II-14)}$$

and :

$$\boldsymbol{F_{HF} = T_{ind}[\rho] + V_{ind}[\rho] + E_{XC}[\rho]} \quad \textbf{(II-15)}$$

With :

Exc[ρ] is the exchange and correlation energy functional, which includes everything that is not known in the system, namely the effects of correlations due to the quantum nature of electrons. This term includes all multi-electronic effects

$$E_{XC}[\rho] = T[\rho] - T_{ind}[\rho] + V[\rho] - V_{ind}[\rho] \quad \textbf{(II-16)}$$

By defining this new functional, the idea of Kohn and Sham is to extract the maximum of information on the kinetic and potential terms, to bring back all that is unknown in a single contribution that we can approximate and thus minimize the error on the total energy. By minimizing (I-14) we obtain Euler's equation:

$$\int \left[\frac{\delta T_{ind}[\rho]}{\delta \rho(r)} + \int \frac{\rho(r'(dr''')'}{|r-r'|} + V_{e-n}(r) + \frac{\delta E_{XC}[\rho]}{\delta \rho(r)} \right] \delta\rho(r)dr = 0 \quad \textbf{(II-17)}$$

With the number of particles constant, we have:

$$\int \delta\rho(r)dr = 0 \quad \textbf{(II-18)}$$

$$V_{eff}[\rho(r)] = V_{e-n}(r) + V_{Hartree}(r) + V_{XC}[\rho(r)] \quad \textbf{(II-19)}$$

The term in parentheses of equation (II-17) is therefore constant. One can then define an effective potential in which bathe the electrons, it is the first equation of Kohn-Sham: Avec le potentiel de Hartree

$$\boldsymbol{V_{Hartree}(r) = c \int \frac{\rho(r')dr'}{|r-r'|} dr'} \quad \textbf{(II-20)}$$

And the exchange and correlation potential defined by:

$$\boldsymbol{V_{XC} = \frac{\delta E_{XC}[\rho]}{\delta \rho(r)}} \quad \textbf{(II-21)}$$

With (II-17) and (II-19) comes the second Kohn-Sham equation which is the system of Ne mono-electronic Schrödinger equations which allows to find the Ne Kohn Sham states Φi(r):

$$\left[-\frac{\hbar^2}{2m_e}\vec{\nabla}^2 + V_{eff}(\vec{r})\right]\Phi_i(r) = \varepsilon_i\Phi_i(r) \quad , \quad i = 1, \ldots\ldots\ldots\ldots, N \qquad \textbf{(II-22)}$$

With εi the Kohn Sham energies. Provided with these states, all that remains is to define the electronic density of the system. This is Kohn Sham's third equation:

$$\rho(r) = \sum_{i=1}^{N_e}|\Phi_i(r)|^2 \qquad \textbf{(II-23)}$$

These three interrelated equations must be solved in a self-consistent manner in order to find the ground state density. All DFT type calculations are based on the iterative resolution of these three equations. Note that for the DFT, only the total energy, the Fermi energy and the electron density have a physical meaning. The states and energies of Kohn Sham are only intermediate calculations. Nevertheless, they are used in many scientific works, to calculate certain quantities such as band structures.

In many cases, for systems where the electrons are poorly correlated, the Kohn Sham states represent a good approximation of the wave function ψe of Ne electrons of the system.

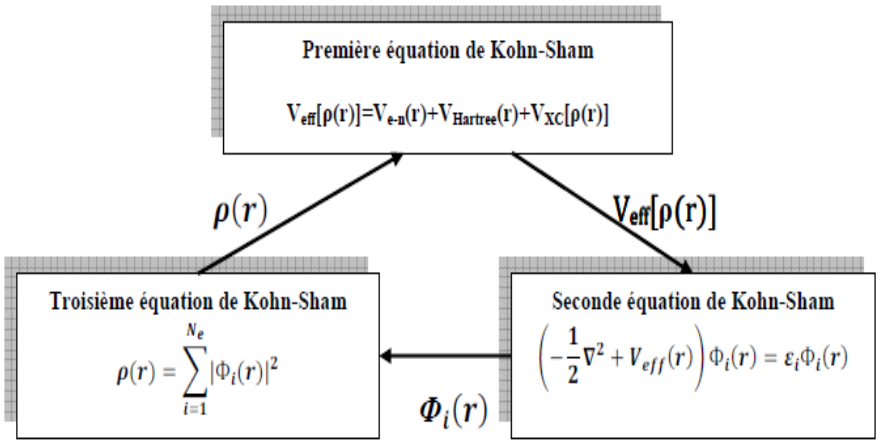

Figure II-1: Interdependence of the Kohn and sham equations.

II-4-3. Exchange and correlation potential:

The exchange and correlation functional must take into account, in addition to the self-consistent calculation, the difference in kinetic energy between the non-interactive fictitious system and the real system. Despite the elegance of the Kohn and Sham (KS) equations, this formulation is unusable without the use of adequate approximations for the exchange and correlation functional EXC.

Thus the calculation of the energy and of the exchange and correlation potential is based on a certain number of approximations, the main ones of which are the LDA and the GGA.

These approximations have aroused the interest of several scientists and recorded enormous progress in this area.

II-4-3-a. LDA local density approximation:

Kohn and Sham proposed in 1965 the local density approximation (LDA) based on the assumption that the terms of exchange and correlation depend only on the local value of ρ. The local density approach [33, 34] is based on the uniform electron gas model. This describes it as**:**

$$\boldsymbol{E_{XC}}\ (\boldsymbol{\rho}) = \int \boldsymbol{\rho \varepsilon_{XC}}\, \boldsymbol{\rho(r) dr} \qquad \textbf{(II-24)}$$

with :

$$\boldsymbol{\varepsilon_{XC}} = \boldsymbol{\varepsilon_{XC}^{homo}} \boldsymbol{\rho(r)} \qquad \textbf{(II-25)}$$

Where ε_XC^homo (ρ) is the exchange and correlation energy per electron belonging to an electron gas of uniform density ρ. There is also a version the LDA which makes it possible to take into account the electronic spin: it is the approximation of the local spin density LSDA. The energy of exchange and correlation E becomes a functional of the two high spin densities and bottom:

$$\epsilon_{XC}^{LSDA}(\rho\uparrow.\rho\downarrow) = \int \rho(r)\varepsilon_{XC}(\rho\uparrow(r).\rho(r)\downarrow)dr \qquad \textbf{(II-26)}$$

As an important remark, two contributions from the exchange and correlation energy of a free electron:

$$\varepsilon_{XC} = \varepsilon_X(r) + \varepsilon_c(r) \qquad \textbf{(II-27)}$$

$\varepsilon_X$est is the exchange energy and ε_(c) is the correlation energy.

In the approximation of the local density, the total energy of exchange and correlation ε_XC (ρ) Is written:

$$E_{XC} = \frac{e^2}{2}\int dr^3 \rho(r)\varepsilon_{XC}\,\rho(r) \qquad \textbf{(II-28)}$$

The correlation energy is when it overestimated, but, since it contributes only weakly to the total energy, the error is small. Since the electron density is considered to be locally uniform, systems for which the density varies abruptly cannot be described correctly.

II-4-3-b . Approximation of the generalized gradient GGA:

The GGA (Generalized Gradient Approximation[35] allows a combination between the local terms depending on the gradient. By using the LDA approximation, we use the knowledge of the density at the point r, whereas in a real system the density is spatially, inhomogeneity consequently, it will be more suitable to introduce a correction to this functional which would take into account the rate of variation of hj: the most natural way to improve the LDA is to take into account the inhomogeneity of the electron density by introducing into the he energy of exchange and correlation of the terms depend on the gradient of the density. This definition of the functional GGA implies that it is of the form:

$$E_{XC}^{GGA}(\rho) = \int \epsilon_{XC}\rho(r)\nabla\rho(r)\rho(r)dr \qquad \textbf{(II-29)}$$

Where ε_(XC) (ρ(r), ∇ρ(r)) represents the exchange and correlation energy per electron in a mutually interacting electron system of uniform nom density. L'avènement de these GGA-like functionals [36-37] is at the origin of the massive use of DFT within the community of chemists in the 1990s. The use of the GGA-like functional indeed

makes it possible to increase significantly has the precision of the calculations compared to the description provided by the LDA, in particular for the binding energy of the molecules.

The order of magnitude of the relative error committed at the level of the atomization energy calculation is lowered to 3-7% when a GGA functional is used while an LDA functional leads to overestimations of the order of 20 -30% [38-39]. The energy barriers and energy difference between two distinct structures [40-41] and has the origin of lengthening and softening the bond.

This last effect strongly corrects [42] the results obtained at the LDA level. GGA-like functionals also provide a better description of equilibrium volumes, moduli of elasticity and magnetic properties of compounds compared to the calculations themselves in the local density approximation.

II-4-4. Solving the Kohn and Sham equations:

Solving the Kohn and Sham equations in general requires choosing a basis for the wave functions which can be taken as a linear combination of orbitals called Kohn-Sham (KS) orbitals these orbitals can be written Under the form:

$$\mathbf{\Psi_i(\vec{r}) = \sum c_{ij}\phi_{j\overrightarrow{(r)}}} \qquad \textbf{(II-30)}$$

Where $\phi_j\left(\vec{r}\right)$ are the basis functions and the series expansion coefficients of. These coefficients $\psi_i\left(\vec{r}\right)$ are the only variables of the problem, since the density depends only on the orbitals of Kohn and Sham. Using the variational principle, solving the Kohn and Sham equations boils down to determining the coefficients Cij for the occupied orbitals that minimize the total energy. Solving the KS equations for the points of symmetry in the first Brillouin zone makes it possible to simplify the calculations.

This resolution is done iteratively using a self-consistent iteration cycle presented by the flowchart of (figure II-2). We start by injecting the initial charge density to diagonalize

the secular equation: Where H represents the Hamiltonian matrix and S the covering matrix.

Then the new charge density is constructed with the eigenvectors of this secular equation using the total charge density which can be obtained by summation over all occupied orbitals (II-23).

If the calculations do not agree, we mix the two densities and in the following way:

$$\boldsymbol{\rho_{in}^{i+1} = (1-\alpha)\rho_{in}^{i} + \alpha\rho_{out}^{i}} \qquad \textbf{(II-31)}$$

i represents the ith iteration and α a mixing parameter. The procedure is continued until convergence is reached.

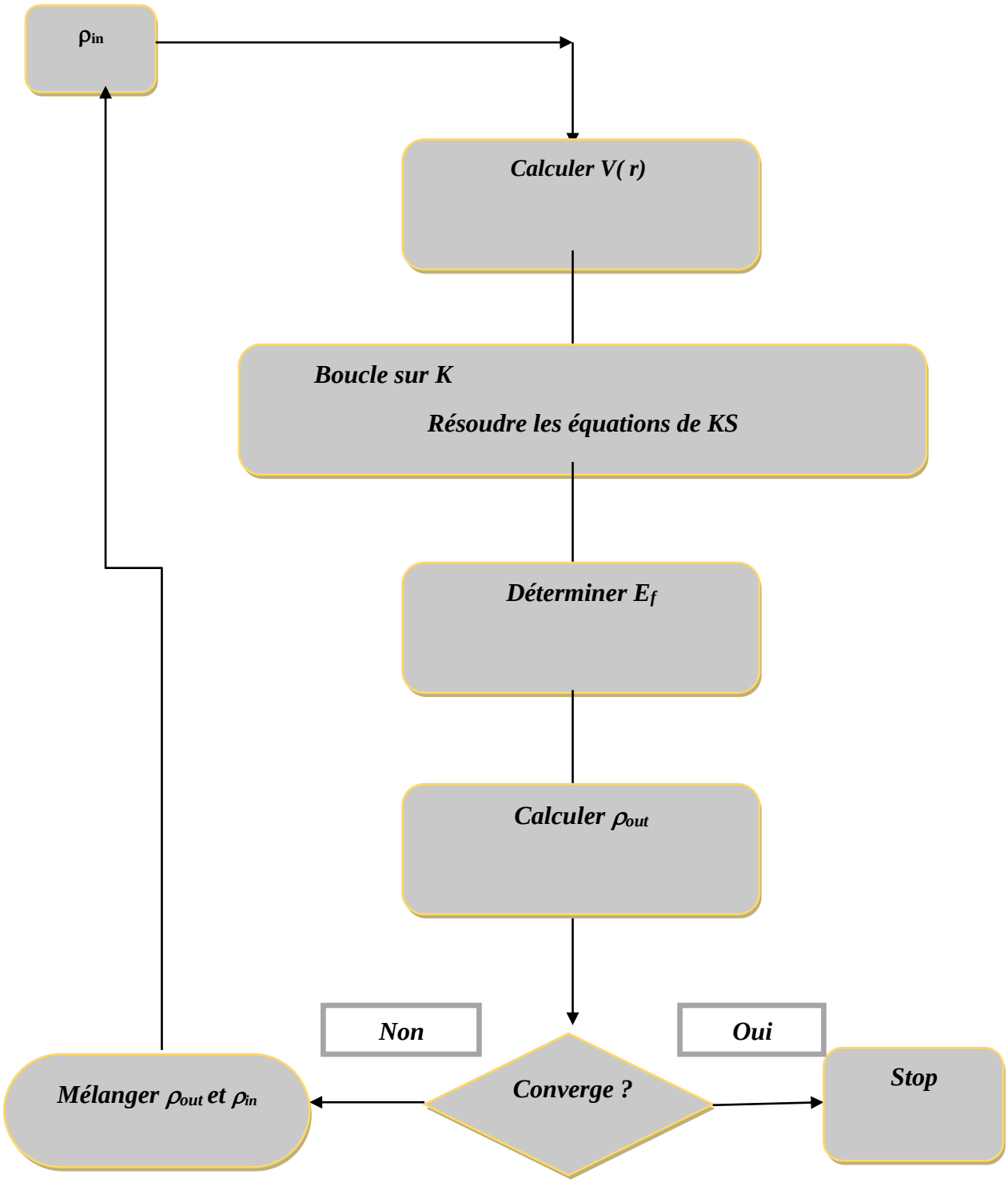

Figure II-2 : diagram of the self-consistent calculus of the Density Functional Theory.

II-5. Conclusion:

In this chapter, we presented the theoretical concept of DFT. It consists in taking into account the multi-body effects by the solution of the Schrödinger equation to a particle in an average field due to the other particles. The formalism of the DFT is based on the theorem of Hohenberg and Kohn (1964), which is based on the consideration that the total energy of a system is a functional of the electron density.

DFT is a quantum theory that produces precise results for solving electronic structures.

Chapter III:

The Linearized Augmented Plane Wave Method (FP-(LAPW

III-1. Introduction:

There are several methods for calculating band structures, which are classified into three main types depending on whether they require experimental results or fundamental data:

- Empirical methods for which the calculations require experimental results.
- Semi-empirical methods for which the calculations require both experimental results and fundamental data.
- Ab-initio methods for which the calculations only require fundamental data.

In recent years, researchers have developed (ab initio) methods based on theoretical concepts known as “First Principal Methods”. All these methods have a single starting point which is the resolution of the Khon and Sham equation in a self-consistent way. Among these methods, we can cite the three most well-known groups in DFT:

- Methods based on a linear combination of atomic orbitals (LCAO) [43,44], usable for example, for the "d" bands of transition metals.
- Methods derived from orthogonalized plane waves (OPW) [44,45] better adapted. to the conduction bands of "s-p" character of simple metals.
- Cellular methods of the augmented plane wave type (APW) [46] and the Green's function method of Korringa, Kohn and Rostoker (KKR) [47, 48] applicable to a greater variety of materials. The linearized methods developed by Andersen [48], Linearized Augmented Plane Waves (LAPW) and Linearized “Muffin-Tin” Orbitals (LMTO), save several orders of magnitude in computation time.

III-2. Linearized augmented plane wave method (FP-LAPW):

The linear augmented plane wave (LAPW) method, developed by Andersen [49], is basically an improvement of the so-called augmented plane wave (APW) method developed by Slater (1937-1964) [45, 50].

III-2-1. Augmented plane wave (APW) meth:

Slater developed in 1937 the new APW (Augmented Plane Wave) method [45] in which he proposed a radial step by the introduction of the Muffin-tin approximation to describe the crystal potential. According to this approximation, the unit cell will be divided into two types of regions:

- The first region is taken near the atomic nucleus, where the potential and wave function are similar to those of an isolated atom. In this space which is defined by a "Muffin-Tin" sphere (RMT) of radius Rα, the potential has a spherical symmetry and the wave functions are radial functions "solution of the Schrödinger equation".
- The second region is the interstitial region (IR), where the potential is considered constant and the wave functions used are plane waves (figure III-1)

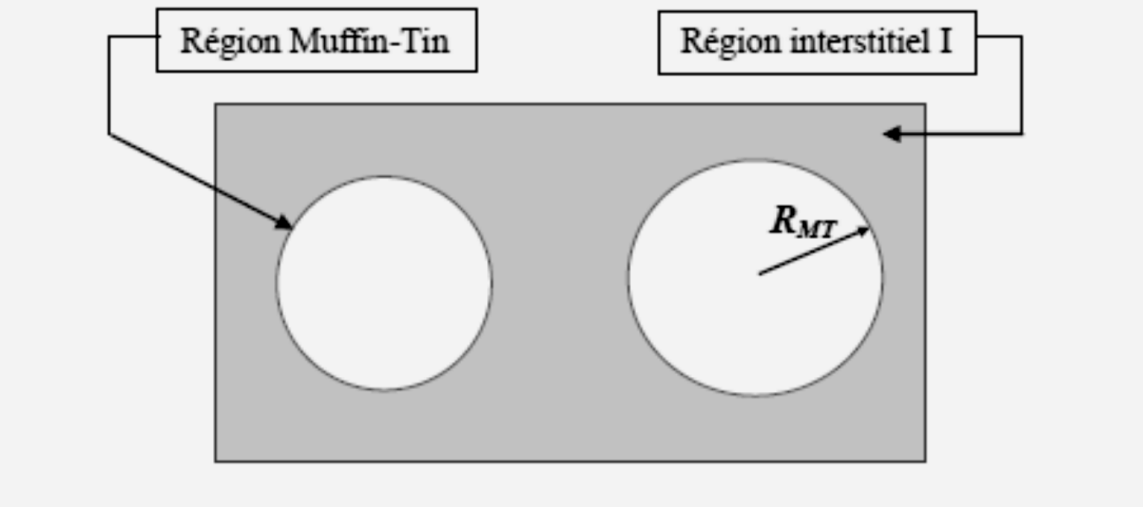

Figure III-1: Representation of Muffin-Tin "RMT" potential.

So, the wave function is written in the form:

$$\Phi(r) = \begin{cases} \frac{1}{\Omega^{1/2}} \sum_G C_G \, e^{i(G+K)r} & r > R_\alpha \\ \sum_{lm} A_{lm} \, U_l(r) Y_{lm}(r) & r < R_\alpha \end{cases} \qquad \textbf{(III-1)}$$

Or:

R_α is the radius of the sphere MT

C_G et A_{lm} the development coefficients.

Ω: Volume of the unit mesh.

Y_{lm}: Spherical harmonics.

$U_l(r)$ is the regular solution of the Schrödinger equation for the radial part and given by:

$$\left\{-\frac{d^2}{dr^2}+\frac{l(l+1)}{r^2}+V(r)-E_l\right\} rU_l(r)=0 \qquad \textbf{(III-2)}$$

when :

E_l is the linearization energy and V(r) is the Muffin-Tin potential.

The radial functions are defined by the previous equation, are orthogonal to any eigenstate of the core, but this orthogonality disappears on the limit of the sphere [10]. As the following equation shows:

$$(E_2-E_1)rU_1U_2=U_2\frac{d^2rU_1}{dr^2}-U_1\frac{d^2rU_2}{dr^2} \qquad \textbf{(III-3)}$$

Where: U1 and U2 are the radial solutions corresponding to the energies E1 and E2, respectively. The overlap is constructed using relation (III-3) and integrating by parts. Slater made a particular choice for wave functions [51-52]. It shows that plane waves are the solutions of Schrödinger's equation in the case of a constant potential, while radial functions are the solutions in the case of a spherical potential, so it proves that El is equal to the own value. This approximation (MT) gives very satisfactory results especially for compact structures (fcc and hcp). For bcc structures, this approximation gives results that are not totally bad but more or less reasonable [53], whereas, in the case where the symmetry sites and the coordinations are weak, this method is not recommended.
To ensure the continuity of the function φ(r) at the surface of the sphere MT, the coefficients Alm must be developed according to the coefficient C_G of the plane waves existing in the interstitial regions. So after the calculations:

$$A_{lm}=\frac{4\pi i^l}{\Omega^{1/2}U_l(R_\alpha)}\sum C_G j_l(|K+g|R_\alpha)Y_{lm}^*(K+G) \qquad \textbf{(III -4)}$$

where the origin is taken at the center of the sphere.

R : is the radius of the sphere.

The A_{lm} are determined by the plane wave coefficients G_C and the energy parameters El. These two terms are variational coefficients in the APW method. The individual functions, labeled by G, thus become compatible with the radial functions in the spheres, and we then obtain augmented plane waves (APW).
Consequently, the energy E_l must be equal to that of the band of index G. This means that the energy bands (for a point k) cannot be obtained by a simple diagonalization, and that it is necessary to treat the secular determinant as a function of the energy.

The method (APW), thus constructed, presents some difficulties related to the function Ul(Rα) which appears in the denominator of equation (III-4). Indeed, depending on the value of the parameter El, the value of Ul (Rα) can become zero at the surface of the sphere MT, leading to a separation of the radial functions with respect to the plane wave functions. In order to overcome this problem, several modifications to the method (APW) have been made, notably those proposed by Koelling [54] and by Andersen [55]. The modification consists in representing the wave function inside the spheres by a linear combination of the radial functions Ul (r) and their derivatives with respect to the energy Ul, thus giving rise to the FP-LAPW method.

III-2-2. Principle of the LAPW method:

The LAPW method [56,57] is a method for solving the Kohnet Sham equations to find the ground state density, total energy and eigenvalues of a multi-electron system, by introducing bases specially adapted to the problem.

In the LAPW method the bases inside the sphere are linear $U_{lm}^{\bullet}(r)Y_{lm}(r)$ combinations of radial functions $U_l(r)Y(r)_{lm}$ their derivatives with respect to l 'energy. The functions U are defined exactly as in the method (APW) with fixed El Equation (III-3). The derivative of Ul with respect to the energy satisfies the following condition

$$: \left\{-\frac{d^2}{dr^2} + \frac{l(l+1)}{r^2} + V(r) - E_l\right\} r U_l^{\bullet}(r) = r U_l(r) \qquad \textbf{(III-5)}$$

In the non-relativistic case, these radial functions Ul and _(U_l)^• ensure, on the surface of the sphere MT, continuity with the plane waves from the outside. The wave functions thus augmented become the basic functions (LAPW) of the method (FP-LAPW):

$$\boldsymbol{\phi}(\boldsymbol{r}) = \begin{cases} \frac{\mathbf{1}}{\Omega^{1/2}} \sum_{\boldsymbol{G}} \boldsymbol{G}_{\boldsymbol{G}} \boldsymbol{e}^{\boldsymbol{i}(\boldsymbol{G}+\boldsymbol{K})\boldsymbol{r}} & \boldsymbol{r} > \boldsymbol{R}_{\boldsymbol{\alpha}} \\ \sum_{\boldsymbol{lm}} [\boldsymbol{A}_{\boldsymbol{lm}} \boldsymbol{U}_{\boldsymbol{l}}(\boldsymbol{r}) + \boldsymbol{B}_{\boldsymbol{lm}} \boldsymbol{U}_{\boldsymbol{l}}(\boldsymbol{r})] \boldsymbol{Y}_{\boldsymbol{lm}}(\boldsymbol{r}) & \boldsymbol{r} < \boldsymbol{R}_{\boldsymbol{\alpha}} \end{cases} \quad \textbf{(III-6)}$$

where: the coefficients B_{lm} correspond to the function $\dot{U}_l$ are of the same nature as the coefficients A_{lm}.

In the (LAPW) method, plane waves are used in the interstitial region as in the case of the APW method. But inside the spheres, linearly augmented plane waves (LAPW's) are used which have more variational freedom than augmented plane waves (APW's) in the (APW) method. The radial functions can be expanded in the neighborhood of El by:

$$\boldsymbol{U}_{\boldsymbol{l}}(\boldsymbol{E}, \boldsymbol{r}) = \boldsymbol{U}_{\boldsymbol{l}}(\boldsymbol{E}_{\boldsymbol{l}}, \boldsymbol{r}) + (\boldsymbol{E} - \boldsymbol{E}_{\boldsymbol{l}}) \boldsymbol{U}_{\boldsymbol{l}}(\boldsymbol{E}, \boldsymbol{r}) + \mathbf{0}((\boldsymbol{E} - \boldsymbol{E}_{\boldsymbol{l}})^{\mathbf{2}}) \quad \textbf{(III-7)}$$

Où $\mathbf{0}((\boldsymbol{E} - \boldsymbol{E}_{\boldsymbol{l}})^{\mathbf{2}})$ indicates the energy squared error.

In this method, the error introduced in the calculation of the function and the energy, is of the order of (E - El)2 and (E-El)4 respectively.

Linearly augmented plane waves (LAPW) form a good basis over a relatively wide energy range. As well, all valence bands can be handled typically with a single value of El.

When the case is not possible, one can generally divide the energy window into two parts, which is a great simplification compared to the (APW) method.

In general, if Ul is equal to zero at the surface of the sphere, its derivative will be different from zero. Consequently, the problem of continuity on the surface of the sphere MT will not arise in the method (LAPW).

III -3. The roles of linearization energies El:

The Ul and functions are orthogonal to any state of the heart that is strictly confined within the MT spheres. Unfortunately, this condition is never satisfied exactly except in the case where there are no core states with the same l. As a result, there will be an extended core states component contained in the valence wave functions. This problem is not dealt with by the APW method, whereas the non-orthogonality of some core states in the FP-LAPW method requires a delicate choice of El. In this case, the calculation cannot be performed without modifying El. The ideal solution in such cases is to use a local orbital expansion. However, this option is not available in all programs, and in this case, one must choose the largest possible radius of the sphere.

Finally, it should be noted that the various Els should be defined independently of each other. The energy bands have different orbitals. For an accurate calculation of the electronic structure, El should be chosen as close as possible to the energy of the band if the band has the same l.

III-4. Development in local orbitals:

The goal of the method (LAPW) is to obtain precise band energies in the vicinity of the linearization energies El [58]. In most materials, it suffices to choose these energies near the center of the bands. This is not always possible and there are materials for which the choice of a single value of El is not sufficient to calculate all the energy bands, this is the case for materials with 4f orbitals [59,60] and transition metals [61,62]. This is the fundamental problem of the semi-core state which is intermediate between the valence state and the core state. To be able to remedy this situation, we resort either to the use of multiple energy windows, or to the use of a development in local orbitals.

III-4-1. The LAPW+LO method:

In this technique, all energy states are treated with a single energy window. Takeda [63], Perta [64], Smrka [65], Shaughnessy [66] and Singh [67] propose a linear combination of two radial functions. The derivatives of these functions with respect to the energy are equal, but the corresponding linearization energies are different.

The eigenfunction has the following form:

$$\phi(r) = \begin{cases} 0 & r > R_{MT} \\ \left[A_{lm}U_l(r, E_{l,l}) + B_{lm}U_l(r, E_{l,l}) + C_{lm}U_l(r, E_{1,2})\right]Y_{lm}(r) & r < R_{MT} \end{cases} \quad \textbf{(III -8)}$$

Where the coefficients C_{lm} are of the same nature as the coefficients A_{lm} and B_{lm} defined previously. Moreover, this modification reduces the error made in the calculation of the conduction and valence bands.

III-4-2.APW+Lo method:

The problem of the method (APW) was the energy dependence of the set of basis functions. This dependency can be discarded in the (LAPW+LO) method at the cost of a larger set of basic functions. Recently, an alternative approach is proposed by Sjösted et al [68] called the APW+lo method. In this method, the set of basis functions will be independent in energy and always has the same size as that of the APW method. In this sense, the APW+lo basis combines the advantages of the APW method and those of the LAPW+LO method. The set of basic functions of "APW+lo" contains the following two types of wave functions:

- The first are augmented plane waves (APW), with a set of fixed energies El:

$$\phi(r) = \begin{cases} \frac{1}{\Omega^{1/2}}\sum_G G_G e^{i(G+K)r} & r > R_\alpha \\ \sum_{lm}\left[A_{lm}U_l(r) + B_{lm}\mathring{U}_l(r)\right]Y_{lm}(r) & r < R_\alpha \end{cases} \quad \textbf{(III-9)}$$

- The second type of functions are local orbitals (lo) different from that of the LAPW+LO method, defined by:

$$\phi(r) = \begin{cases} 0 & r > R_\alpha \\ \sum_{lm}\left[A_{lm}U_l(r, E_l) + B_{lm}\mathring{U}_l(r, l)\right]Y_{lm}(r) & r < R_\alpha \end{cases} \quad \textbf{(III-10)}$$

In a calculation, a mixed basis LAPW and APW+lo can be used for different atoms and even for different values of the number l. In general, one describes the orbitals which converge more slowly with the number of plane waves (like the 3d states of transition metals), or else the atoms having a small sphere size with the base APW+lo and the rest with a base LAPW [69].

III-5. Concept of the FP-LAPW method:

In the method of Full Potential Linearized Augmented Plane Waves (FP-LAPW) [70] no approximation is made for the shape of the potential or the charge density. Rather, they are developed enharmonic of the lattice within each atomic sphere, and in Fourier series in the interstitial regions. This is the origin of the name "Full-Potential".
This method therefore ensures the continuity of the potential at the surface of the sphere MT and develops it in the following form

$$V(r) = \begin{cases} \sum_{lm}(r) Y_{lm}(r) & \text{à } l'intérieure\ de\ la\ sphére \\ \sum_{k}^{lm} V_k\, e^{ikr} & \text{à } l'extérieure\ de\ la\ sphére \end{cases} \quad \textbf{(III-11)}$$

In the same way, the charge density is developed in the form:

$$\rho(r) = \begin{cases} \sum \rho_k e^{ikr} & r > R_\alpha \\ \sum_{lm}^{k} \rho_{\ lm}(r)\, Y_{lm}\,(r) & r < R_\alpha \end{cases} \textbf{(III-12)}$$

The FP-LAPW method offers a complete description of the electron potential and density in all regions of space. This is why it has become the most suitable method for calculations in WIEN2K code.

III-6. Wien2k code:

The Wien2k code is an implementation of the FP-LAPW method. This program was developed by Blaha and his collaborators [71]. Its applications are numerous, such as electric field gradient [72,73], high temperature superconducting systems [74], minerals [75], transition metal surfaces [76] and non-ferromagnetic oxides [78].

The Wien2k code consists of several independent programs linked by the C-SHELL SCRIPT. The use of the different programs is presented in (figure III-2). The calculation is done in three steps:

III-6.1.Initialization:

- **NN**: gives the distances between nearest neighbors and helps to determine the radius of the Muffin-Tin sphere.
- **LSTART**: generates the atomic densities and determines how the different orbitals are treated in the calculation of the band structure (i.e. core states and valence states, with or without local orbitals…).
- **SYMMETRY**: Generates the space group symmetry operations, determines the point group of individual atomic sites, generates the LM expansion for the lattice harmonics, and determines the local rotation matrices.
- **KGEN**: generates a mesh k in the Brillouin zone.
- **DSTART**: generates a starting density for the SCF cycle by superimposing the atomic densities generated in LSTART.

III-6.2.SCF calculation:

- The SCF cycle includes the following steps:
- **LAPW0**: generates the potential from the density.
- **LAPW1**: calculates the valence bands (eigenvalues and eigenvectors)
- **LAPW2**: calculates the valence densities from the eigenvectors.
- **LCORE**: calculates core states and densities.
- **MIXER**: mixes the valence and core densities to produce a new density.

Calculation of properties:

The calculation of the physical properties is done using the programs:

- **OPTIMISE**: determines the total energy according to the volume which is used to calculate the parameter of the network, the module of compressibility and its derivative.
- **TETRA**: calculates the total and partial state density.

- **SPAGHETTI**: calculates the band structure using the eigenvalues generated by LAPW1.
- **OPTIC**: calculates the optical properties.
- **XSPEC:** calculates the structures of the absorption and emission spectra of X-rays.

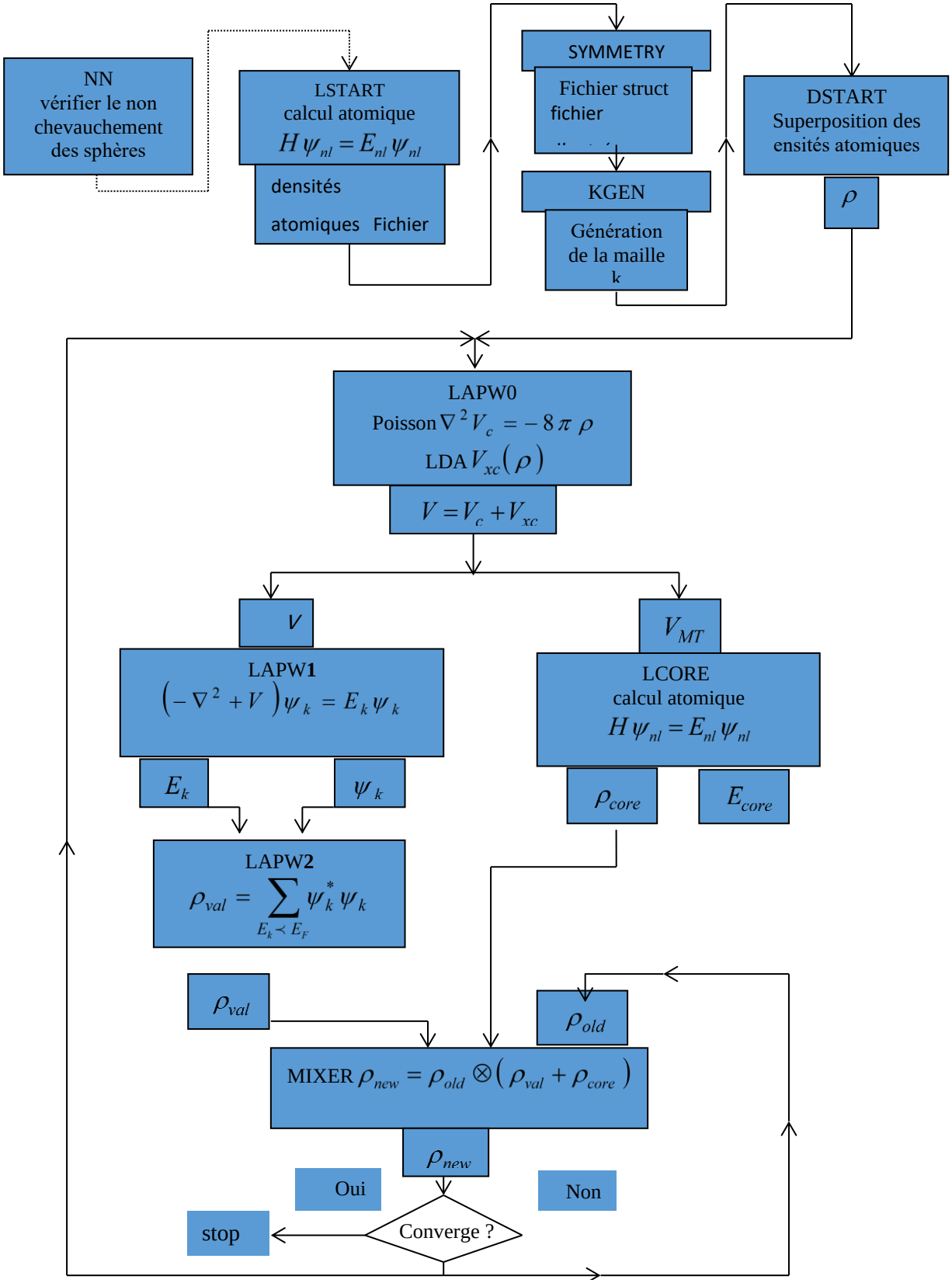

Figure III-2: The Wien2k code

III-7. Conclusion:

The Wien2k is a “Full-Potential Linearized Augmented Plane Wave” code which makes it possible to study an infinite and periodic crystal. The FP-LAPW method consists of partitioning the space into two parts:

- a region inside atomic spheres (Sα) which surround the nuclei (of index α) and do not overlap.
- the region outside the spheres, called the interstitial region (I).

In this chapter we have described this FP-LAPW method in detail. The goal of all this is to find the best compromise between a detailed description of the systems, in terms of model and methodology, and reasonable computation times, thus allowing a broader exploration of the problem studied.

Chapter 4: Results and discussion

IV-1. Introduction:

The main objective of our research work is the prediction of the physico-chemical properties of solid materials. Several theoretical models have been proposed in order to interpret recent experimental measurements on the one hand, and on the other hand to predict new materials. Grasse to an ab-initio method, in this case the augmented and linearized plane wave method (FP-LAPW) we studied in detail the fundamental properties of the MgGeAs2 and MgSiAs2 compounds. It is for this reason that we will present the main properties of the ternary compounds MgGeAs2 and MgSiAs2. We analyze and interpret the results concerning the structural, electronic and optical properties. The results obtained are discussed and compared with those of the experimental and with other theoretical calculations available in the literature.

IV-2. Calculation details:

The present work was carried out using the augmented and linearized plane wave method (FP-LAPW) [79] implemented in the Wien2k code [80], it is an ab-initio method based on the formalism of the theory of density functional (DFT) [81, 82]. Our work consists in calculating the structural, electronic and optical properties of the ternary compounds MgGeAs2 and MgSiAs2.

For the treatment of the exchange and correlation potential, the generalized gradient approximation developed by Wu-Cohen (WC-GGA) [83] was used for the optimization of the structural parameters. For the electronic properties, in addition to the WC-GGA approximation, the recent approximation proposed by Becke and Johnson (mBJ: modified Becke-Johnson)[84] was also used.

This approach has been developed with the aim of improving the values of the energy gaps which are often underestimated by the already known approximations and consequently the problem of the failure of the DFT for the excited states can be solved. In the FP-LAPW method, the space is divided into two regions; non-overlapping spheres surrounding the atomic sites of RMT rays (Muffin-Tin) and an interstitial region. In the first region, the basis functions, the electronic densities and the potentials are developed in combination of spherical harmonics up to a value of lmax=10, on the other hand in the interstitial region, they are developed in Fourrier

series with a cut-off radius RMTKmax= 8 where RMT is the smallest radius of the sphere MT (kmax is the norm of the largest wave vector used for the plane wave development of the eigenfunctions).

Muffin-Tin radii (RMT) were taken as 2.0, 2.0, 2.0, 2.0 a.u. for Mg, Ge, Si and Te atoms respectively. The separation energy between core states and valence states is chosen

equal to -6 Ry. The self-consistent calculations are considered to have converged when the total energy is stable at 0.1 mRy.

IV-3. Study of ternary chalcopyrite's:

IV-3-1. Structural properties:

This first part is the most important step in all the theoretical calculations. The determination of structural parameters is considered as a starting point for other physical properties in general. The structural parameters such as the lattice parameters a0, c0, the modulus of compressibility B0 and its derivative B0' can be determined either experimentally by the use of X-ray diffraction (XRD) techniques, or theoretically via the use of computer simulation techniques. The latter is used in our calculations using the code wien2k_18.

The calculation of the structural properties is carried out in three successive stages as follows:

- The creation of the structural file (Struct-Gen):
  In this step, the structure is defined by creating a basic file which consists of the microscopic indications of the chalcopyrite material (the number of atoms, the type of mesh, the spatial symmetry group, the lattice parameter, the positions atomic numbers and the muffin-tin radius of each atom).
- Initialization: It is a sequence of programs which consists in checking: the overlap between the atoms, the symmetry, the energy of separation between the core states and the valence states, as well as the determination of RMTKMAX, the number of points k, the type of the exchange and correlation potential as well as the calculation of the starting density (DSTART).
- Optimization: this operation consists of four steps as follows:
  - Optimization of the volume with constant c/a: in fact this optimization consists in varying the total energy (Etot) according to
  the volume (V) of the primitive cell (compression and dilation). This step makes it possible to obtain the equilibrium volume.
  - Optimization of c/a with constant V: in this optimization, the energy is varied according to c/a. Then, the curve obtained is fitted to a quadratic function.
  - Optimization of u: allows to obtain the parameter u using the command min position.
  - Optimization of the volume: again we calculate the energy according to the volume, which allows us to find the parameter of the cell at equilibrium and the modulus of compressibility as well as its first derivative. For this, the Etot points (V) calculated are adjusted to the Murnaghan equation of state [85] which is given by the following equation:

$$E(V) = \frac{B_0 V}{B_0'}\left[\frac{(V_0/V)^{B_0'}}{B_0'-1} - 1\right] + E(V_0) - \frac{B_0 V}{B_0'-1} \qquad \textbf{(IV-1)}$$

(V): ground state energy as a function of cell volume V.

$\mathbf{B_0}$: Equilibrium compressibility modulus.

$\mathbf{V_0}$: Balance volume.

$\mathbf{B_0'}$: Derived from the modulus of compressibility at equilibrium.

The parameters of the cell at equilibrium are deduced from the minimum of the Etot curve the modulus of compressibility $\mathbf{B_0}$ is determined by:

$$B_0 = V\frac{\partial^2 E}{\partial V^2} \qquad \textbf{(IV-2)}$$

In the figure (IV.1), we have represented the variation of the total energy as a function of the volume of the MgGeAs2 and MgSiAs2 compounds using the WC-GGA approximation.

The values obtained for the mesh parameter and the modulus of compressibility are given in the table (IV-1) the experimental and theoretical results are summarized in the same table to compare them with ours. According to the table (IV-1), we note that the values of the lattice parameters of the compounds MgGeAs2 and MgSiAs2 are close to those measured experimentally and calculated theoretically. For the modulus of compressibility, we note the absence of experimental data.

Therefore, the values obtained are predictions and can serve as a reference for future work on these materials. In conclusion, we can say that the values of the structural parameters (a and c) obtained on the one hand are in very good agreement with those found experimentally and on the other hand are better than the theoretical values available in the literature compared to the experience. This improvement of the results is due to the use of the approximation, (WC-GGA) which proved to be very efficient for the calculation of the structural parameters compared to the other GGA functionals.

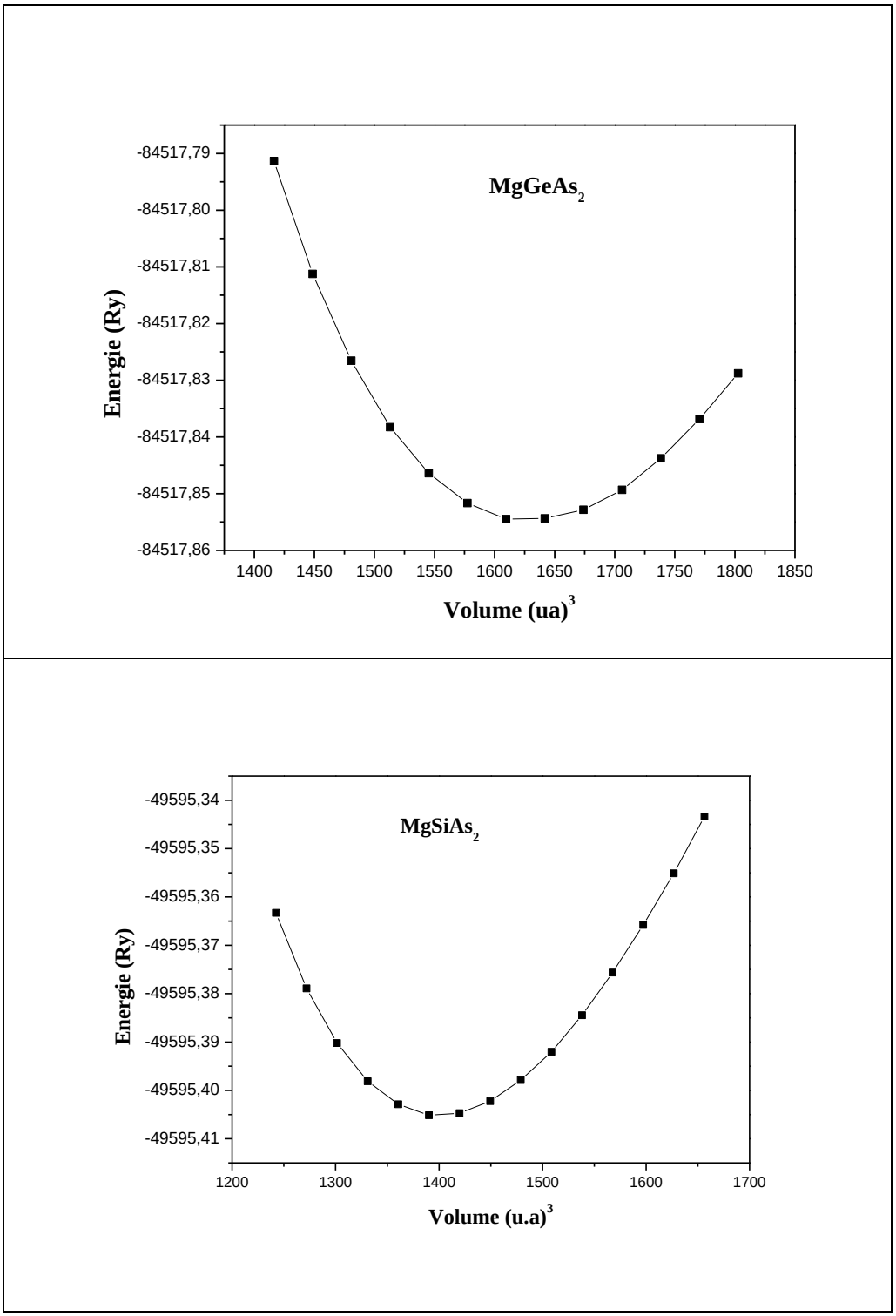

Figure IV-1: Variation of total energy as a function of volume for MgGeAs2 and MgSiAs2 compounds.

Table IV-1: Lattice parameters (a, c) (Å), compressibility modulus B (GPa), and its derivative B' of the compounds MgGeAs 2 and MgSiAs 2 .

Composées		*a (A^0)*	*c (A^0)*	*c/a*	*B(GPa)*	*B'*
$MgSiAs_2$	**Nos calculs**	5.874	10.847	1.8466	60.0960	4.2909
	Exp	5.94[a]	10.59[a]	1.7810	-	-
	Autres calculs	5.954[b]	10.800[b]		63.109[b]	4.19[b]
$MgGeAs_2$	**Nos calculs**	5.991	11.03	1.8410	55.4479	4.399
	Exp	[a]6.009	[a]11.27	-	-	-
	Autres calculs	5.841[b]	11.03[b]		58.85[b]	4.4[b]

aRef bRef [18].

[a][18], V L Shaposhnikov, A V Krivosheeva, V E Borisenko, J L Lazzari and F Arnaud d'Avitaya, Phys. Rev. B 85, 20520 (2012).

[b][18], B Kocak and Y O Ciftci, Mater. Res. Bull. 77, 300 (2016).

IV-3-2. Electronic properties

IV-3-2-1.Band structure

In this part related to electronic properties, we have calculated band structures along high symmetry directions in the first Brillouin zone of a chalcopyrite structure of MgGeAs2 and MgSiAs2 compounds using WC-GGA, mBJ approximations. The calculation of this type of properties is carried out using the theoretical lattice parameter obtained from the calculations carried out in the structural properties section.

The band structure calculation in the wien2k code runs in four steps:

- Creation of struct file: defined in section (IV.3.1.1).
- Initialization: defined in section (IV.3.1.1).
- Calculation of the scf cycle: the scf cycle is executed (self-consistent or self-consistent cycle) by the run_scf command which gives us the calculated total energy.
- The creation of tape structures: this step is carried out from the Tasks command.

Figure (IV-2) represents the electronic band structures along the high symmetry directions of the Brillouin zone associated with the chalcopyrite structure, using the mBJ approximation. We note from our calculations that the shape of the energy bands is independent of the approximation used, and that the difference lies in the displacement of the bands which is translated by the change in the value of the gap according to the approximation used. For both compounds, the valence band maximum and the conduction band minimum lie at the same symmetry point Γ of the first Brillouin zone, so these compounds are Γ-Γ direct gap semiconductors. The numerical values of the energy gaps calculated by the different functionals for the compounds considered are grouped in the table (IV.2), which also contains other experimental and theoretical results in order to compare them with ours. It is also important to mention that the functional WC-GGA underestimates the value of the energy gap compared to the experiment, this behavior is common to the DFT methods, the latter is well designed for the calculation of the equilibrium properties but it reproduces badly the excited states such as the gap. This behavior is due to the fact that

the approximations used have simple forms which are not sufficient to reproduce the exchange and correlation energy exactly. Engel and Vosko have proposed a new form of the GGA functional which better reproduces the exchange potential and thus improves the values of the energy gaps, but the results remain insufficient and are still far from the experiment. This is well verified in Table IV.2 for the two compounds studied where the values of the gaps are improved compared to WC-GGA, but remain low compared to those measured experimentally. However, the significant improvement is that given by the mBJ where we note the good agreement of our results with those of the experiment. Based on these calculations, we show that the mBJ approach gives better gaps compared to other DFT functionals, it is as efficient as the functional hybrids such as GW (Green wave) which are known for their precision in the calculation of gaps. For this reason, this approximation is a very efficient method in the calculation of energy gaps

and can be used for a wide range of semiconductors. There is an acceptable agreement between the values of our calculated gaps, obtained using the augmented and linearized plane wave method at full potential, and those calculated using theoretical methods. Also, from the table (IV.2), we see that the gap values in both approximations decrease when the atomic number increases, i.e. the gap energy Eg(MgGeAs2) is greater than

Eg(MgSiAs2); this is related to the delocalization of valence electrons as the peripheral electrons move away from the nucleus.

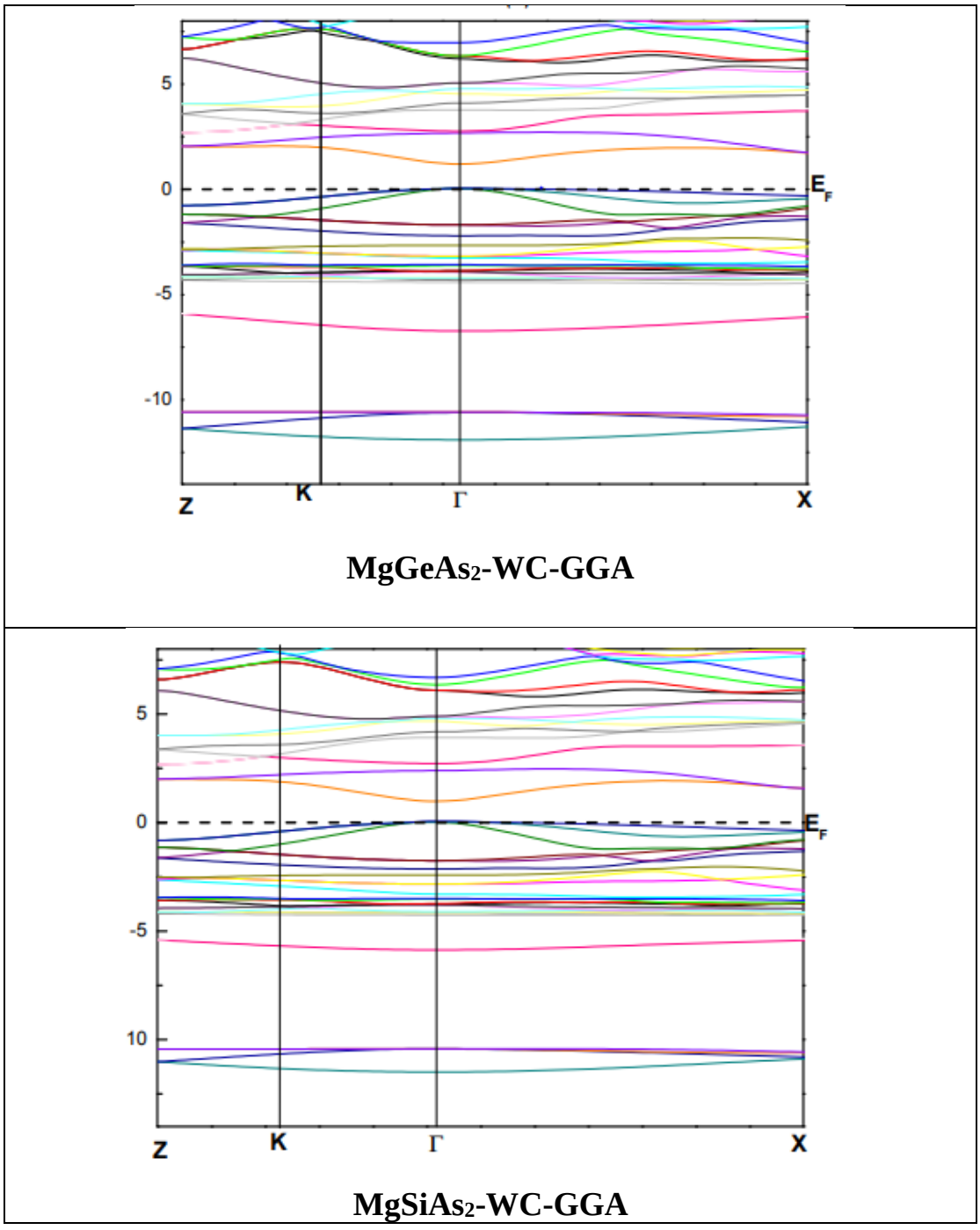

Figure IV-2: Band structure of compounds (a) MgGeAs2 and (b) MgSiAs2 using the mBJ approximation.

Table IV-2: Values of the gap energies (Eg) of its compounds MgGeAs2 and MgSiAs2

E_g (eV) ($\Gamma - \Gamma$)				
	Nos calculs		Expérimentale	Autre calculs
	WC-GGA	mBj		
$MgSiAs_2$	1.32	2.01	2.08[a]	1.95[c]
$MgGeAs_2$	1.04	1.42	1.06[b]	1.39[d]

[a]**Ref [87],** [b]**Ref [88],** [c]**Ref [89] and** [d]**Ref [90].**

[a]**Ref [91]** F Chiker, Z Kebbab, R Miloua and N Benramdane, Solid State

Commun. 151, 1568 (2011)

[b]**Ref [92]**V L Shaposhnikov, A V Krivosheeva, V E Borisenko, J L Lazzari and F Arnaud d'Avitaya, Phys. Rev. B 85, 20520 (2012)

[c]**Ref [93]** J E Jaffe and A Zunger, Phys. Rev. B 29, 1882 (1984)

[d]**Ref [94]** Zh Zhaochun, P Ruiwu and C Nianyi, Mater. Sci. Eng. B 54, 149 (1998).

IV-3-3. Optical properties:

IV-3-3-1 Theoretical reminder:

The physics of semiconductors consists in studying, among other things, the optical properties of materials with a view to their primordial roles in the technology of electronic and optoelectronic components. The optical properties appear during the interaction between the electromagnetic wave and the matter, that is to say when the semiconductor is subjected to an external disturbance such as light.

Many optical phenomena take place when the material is traversed by light radiation, such as absorption, reflection, refraction, diffusion, transmission and emission... and to better understand these phenomena we will study the dielectric function in the context of of quantum mechanics, then we will see the existing link between the real part and the imaginary part of the dielectric function, as well as the complex index through the equations of Kramers – kronig.

IV-3-3-2 Dielectric function

The dielectric function is written in the form $\varepsilon(\omega) = \varepsilon 1(\omega) + i\varepsilon 2(\omega)$, it makes it possible to describe the optical properties of the media for all photons of energy $E=\hbar\omega$ where the

imaginary part ε_2 (ω) of this dielectric function is frequency dependent and it is directly related to the electronic band structure and can be determined by summing all possible transitions from occupied to empty states using the following expression [95]:

$$\boldsymbol{\varepsilon_2(\omega) = \frac{4\pi^2 e^2}{m^2\omega^2}\sum_{i,j}|\langle i|M|j\rangle| * f_i(1 - f_i(\omega) - h\omega)d^3k} \qquad \textbf{(IV-3)}$$

The integral is carried out on the first Brillouin zone, the elements of the dipole moment are given by $\boldsymbol{rM_{cv}(k) = \langle u_{ck}|e\nabla|u_{vk}\rangle}$ from where e is a potential vector which expresses the electric field.

The matrix element $\boldsymbol{M_{cv}(k)}$is a product that represents the direct transition between the valence band states $\boldsymbol{u_{vk}(r)}$ and the conduction band states $\boldsymbol{u_{ck}(r)}$. The energy term $\boldsymbol{\hbar\omega_{cv}(k) = E_{ck} - E_{vk}}$ is the energy corresponding to this transition.

The real part $\varepsilon_1(\omega)$ is derived from the imaginary part of the dielectric function by the Kramers–Kronig transformation according to the following relationship:

$$\boldsymbol{\varepsilon_1(\omega) = 1 + \frac{2}{\pi}P\int_0^{\infty}\frac{\varepsilon_2(\omega')\omega' d\omega'}{\omega'^2 - \omega^2}} \qquad \textbf{(IV-4)}$$

Where ω is the frequency, P is the principal part of the Chauchy integral.

IV-3-3-3 Refractive index:

Another important complex quantity linked to the dielectric function is used to describe the medium, it is the refractive index which is given by the relation**:**

$$\boldsymbol{n(\omega) = \frac{1}{\sqrt{2}}\left[\sqrt{\varepsilon_2^2(\omega) + \varepsilon_2^2(\omega)} + \varepsilon_1(\omega)\right]^{1/2}} \qquad \textbf{(IV-5)}$$

When the frequency vanishes (ω= 0), the equation (IV. 4) is simplified by $\boldsymbol{n(0) = \varepsilon^{1/2}(0)}$**.** .

The knowledge of the real part and the imaginary part of the dielectric function is important in order to be able to determine the refractive index. Other theoretical and empirical models are widely used to estimate the refractive index, among these models we will focus in this study on the following models:

1) The expression proposed by Ravindra et al [96]:

$$\boldsymbol{n = \alpha + \beta E_g}$$

And: **α = 4.084 et β= 0.62**

2) The empirical relationship of Herve and Vandamme [19]:

$$n = \sqrt{1 + \left(\frac{A}{E_g + B}\right)^2}$$

And: **A= 13.6 eV et B= 3.4 eV**

3) Reddy and Nazeer proposed an empirical relationship in the form [89]:

$$n = -\ln 0.102\ \Delta\chi^2$$

Or the electron-negative term, $\Delta\chi^2$ is directly related to the gap: $\Delta\chi^2 = 0.2688\Delta E_g$

IV-3-3-d Absorption coefficient:

The absorption coefficient α(ω) corresponds to the energy addressed per unit of time, volume and divided by the energy flow. It is defined by the following equation:

$$\boldsymbol{\alpha(\omega) = \frac{4\pi}{\lambda} k(\omega)} \qquad \textbf{(IV-6)}$$

$\alpha(\omega)$ is linked to ε_2 by the relation:

$$\alpha(\omega) = \frac{\varepsilon_2(\omega)\omega}{n(\omega)c} \qquad \textbf{(IV-7)}$$

IV-3-3. E Presentation of results and discussion:

The determination of the optical properties was carried out by the use of the WC-GGA approximation with an optimized lattice parameter in the calculations of the structural properties. We chose a number of 1500 k-points in the Brillouin zone, to scan all the optical transitions. Subsequently we plotted all the optical constants in an energy range from 0 to 40 eV. The calculation of the optical properties in the wien2k code is executed only by the progression of the following commands:

- Creation of struct file: defined in section (IV.3.1.1).
- Initialization: defined in section (IV.3.1.1).
- Calculation of the scf cycle: defined in section (IV.3.1.2).
- The Optic command: calculates the components of the dipole moment matrix.
- The joint command: performs the calculation of the imaginary part ε2(ω).
- The Kram command: calculates the real part) using the Kramers-Kronig relations. This is why it is called the Kram command.

A-Imaginary part of the dielectric function:

The variation of the imaginary part of the dielectric function as a function of energy is shown in Figure IV-3 for the compounds MgGeAs2 and MgSiAs2 respectively, for radiation up to 40 eV.

We can first note that the first critical points of the dielectric function that correspond to the fundamental absorption thresholds start at about 0.202 and 0.485 for MgGeAs2 and MgSiAs2, respectively.

The values of the critical points correspond to the transition (direct optical gaps) between valence band and conduction band (Γv-Γc). The main peak, which reflects the absorption maximum, is located at 5.89eV and 1.423 eV for the compounds MgGeAs2 and MgSiAs2 respectively. We also note in these spectra, the presence of secondary peaks around the main peak. For example, in the spectrum of the compound MgGeAs2, the second is the main peak, it is centered around the value 1.913 eV. The third peak is located at 3.87eV, the fourth peak is positioned at 4.68eV. For the compound MgSiAs2, the second is the main peak, it is centered around the value 3.264 eV. The third peak is located at 4.87eV. secondary peaks due to indirect transitions.

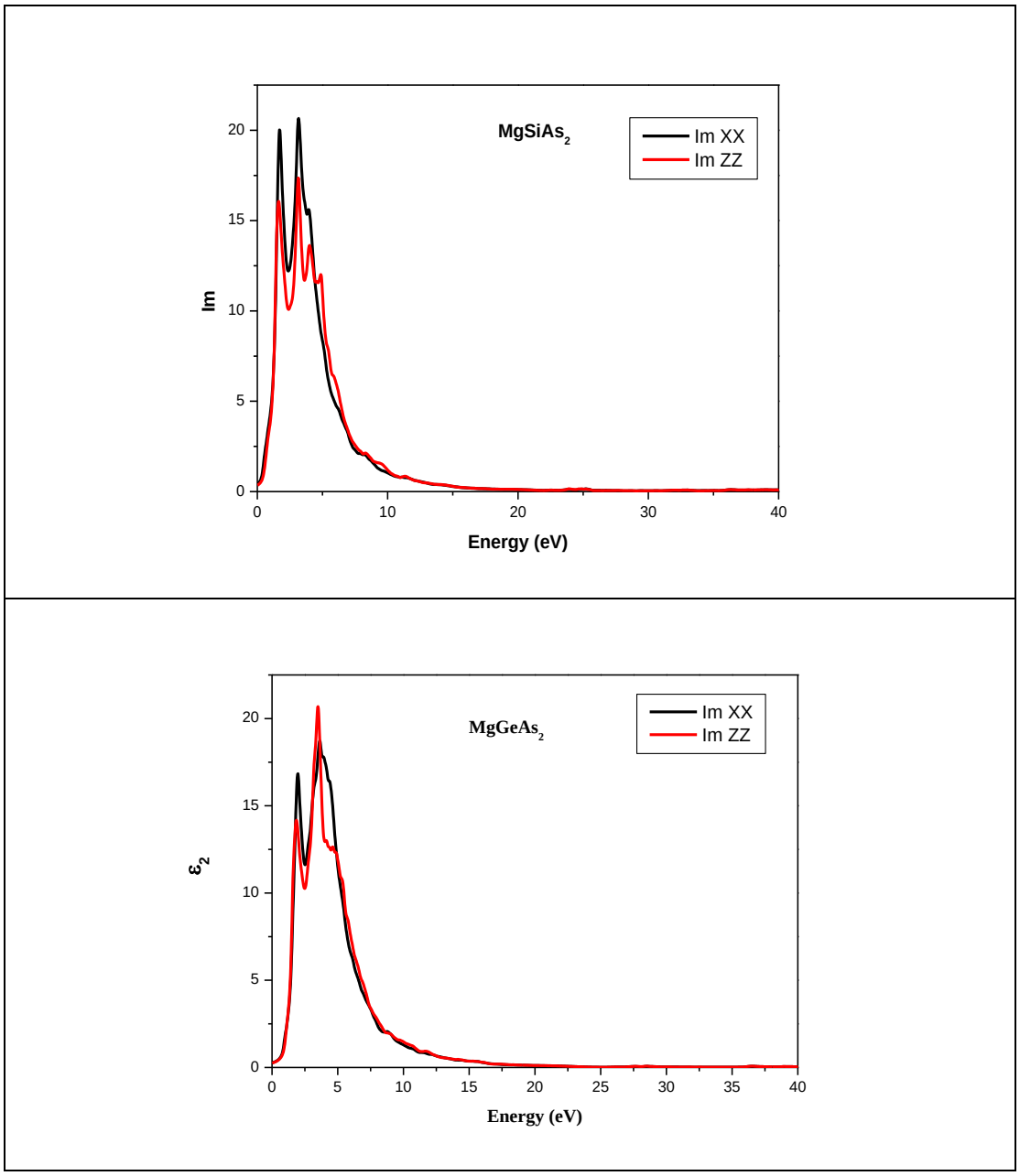

Figure IV-3: Variation of the imaginary parts of the spectrum of the electronic dielectric function ε2(ω) as a function of energy for the compounds MgGeAs2 and MgSiAs2.

B-Real part of the dielectric function:

Figure (IV-4) illustrates the variation of ε1 as a function of energy for MgGeAs2 and MgSiAs2 compounds between 0 and 40 eV. In general, we see that the spectra look almost the same, with small differences. We noticed that for all these compounds the

function ε1(0) vanishes at the following energy values: 11.87 (MgGeAs2) and 15.08 (MgSiAs2). It should be noted that at these energy values the dispersion is zero and therefore the absorption is maximum.

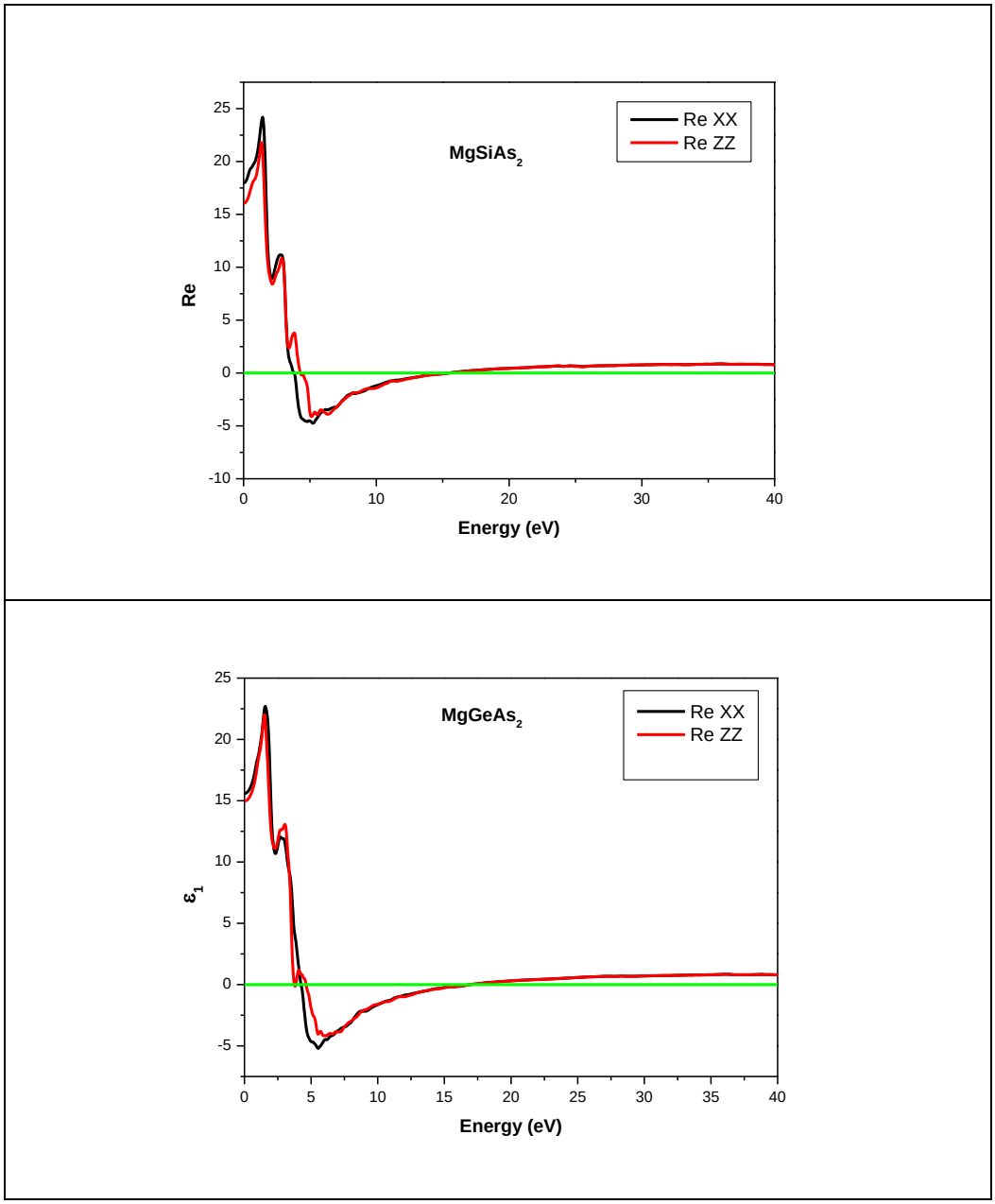

Figure IV-4: Variation of the real parts of the spectrum of the electronic dielectric function ε1(ω) as a function of energy for the compounds MgGeAs2 and MgSiAs2.

Refractive index:

The variation of the refractive index as a function of energy for the four compounds is represented in the figure (IV-5). The curves present a maximum at energies 3.51 and 4.03eV for the compounds MgGeAs2 and MgSiAs2 respectively these main peaks due to the transitions of electrons from the valence band to the conduction band. On the other hand, the static values of the dielectric function $\varepsilon_1(0)$ and of the static refractive index n(0) are reported in Table IV-3 which also contains experimental and theoretical data. It can be seen that the calculated values of $\varepsilon_1(0)$ and n(0) agree well with the theoretical data if we take into account the exchange and correlation energy used in the different approximations.

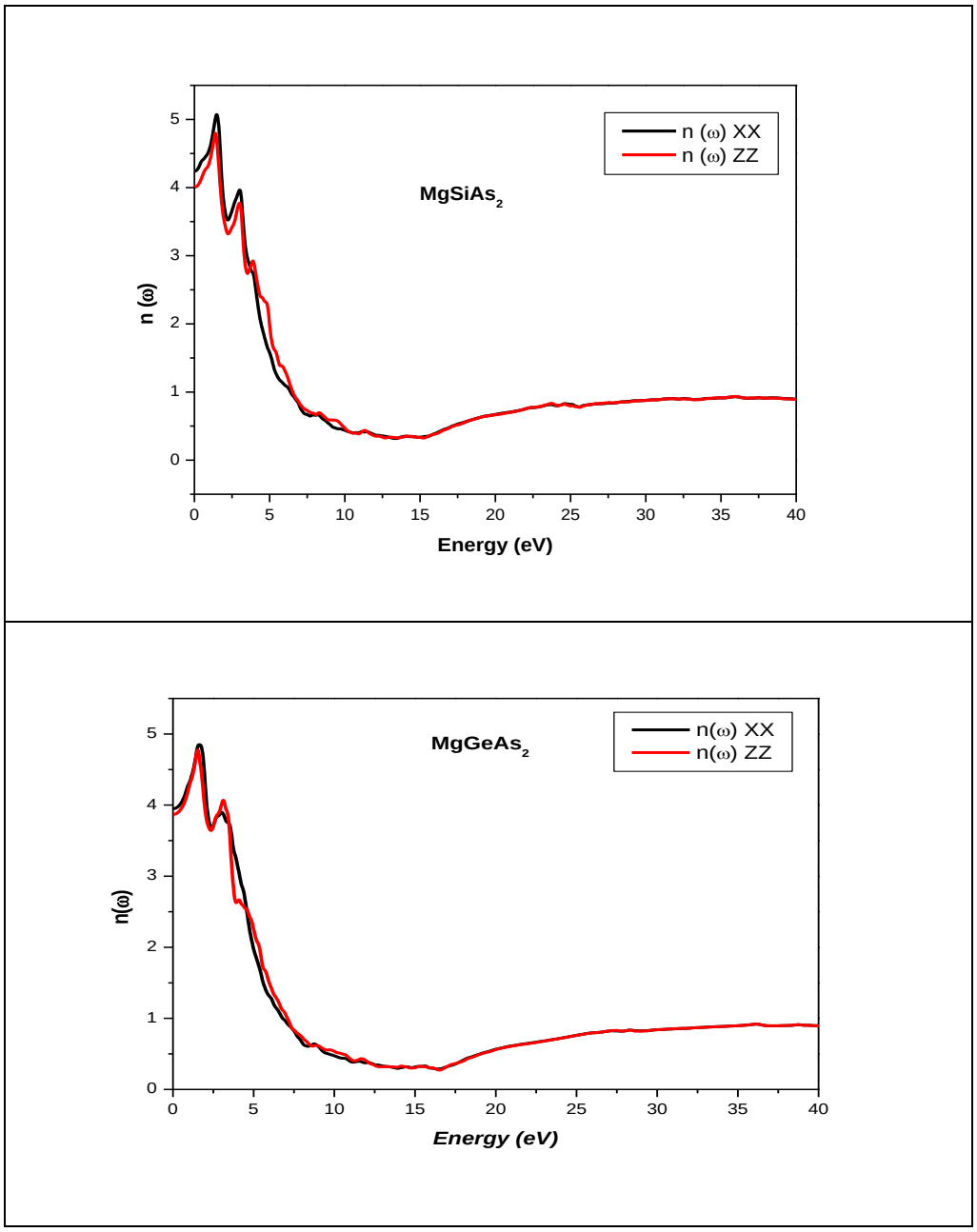

Figure IV-5: Variation of the refractive index n (ω) as a function of energy for MgGeAs2 and MgSiAs2.

Tableau IV-3 : : The static dielectric function ε1(0) and the static refractive index n(0) calculated for the compounds MgSiAs2 and MgGeAs2

	n (0)		$e_1(0)$	
	Nos calculs WC-GGA	**Autre calculs**	**Nos calculs WC-GGA**	**Autre calculs**
$MgSiAs_2$	**4.03**	**4.96[a]**	**17.25**	**17.97[a]**
$MgGeAs_2$	**3.91**	**4.005[b]**	**15.36**	**16.14[b]**

[a]Ref [97], [b]Ref [98].

[a]Ref [99] B Kocak and Y O Ciftci, Mater. Res. Bull. 77, 300 (2016)

[b]Ref [100] F Boukabrine, F Chiker, R Miloua, Z Kebbab, R Khenata, Deo Prakash, S Bin Omran and K D Verma, Opt. Mater. 54, 200 **(2016)**

D- The reflectivity spectrum

The evolution of the reflectivity of the compounds studied is shown in Figure IV-6. According to the spectra the value of the reflectivity in the energy interval (0-40) eV. The curves indicate a maximum of 48% at 9.84eV for MgGeAs2 compounds and 49% at 8.02 eV for MgSiAs2. These results show that our ternary compounds are a priori good candidates for use in the visible range.

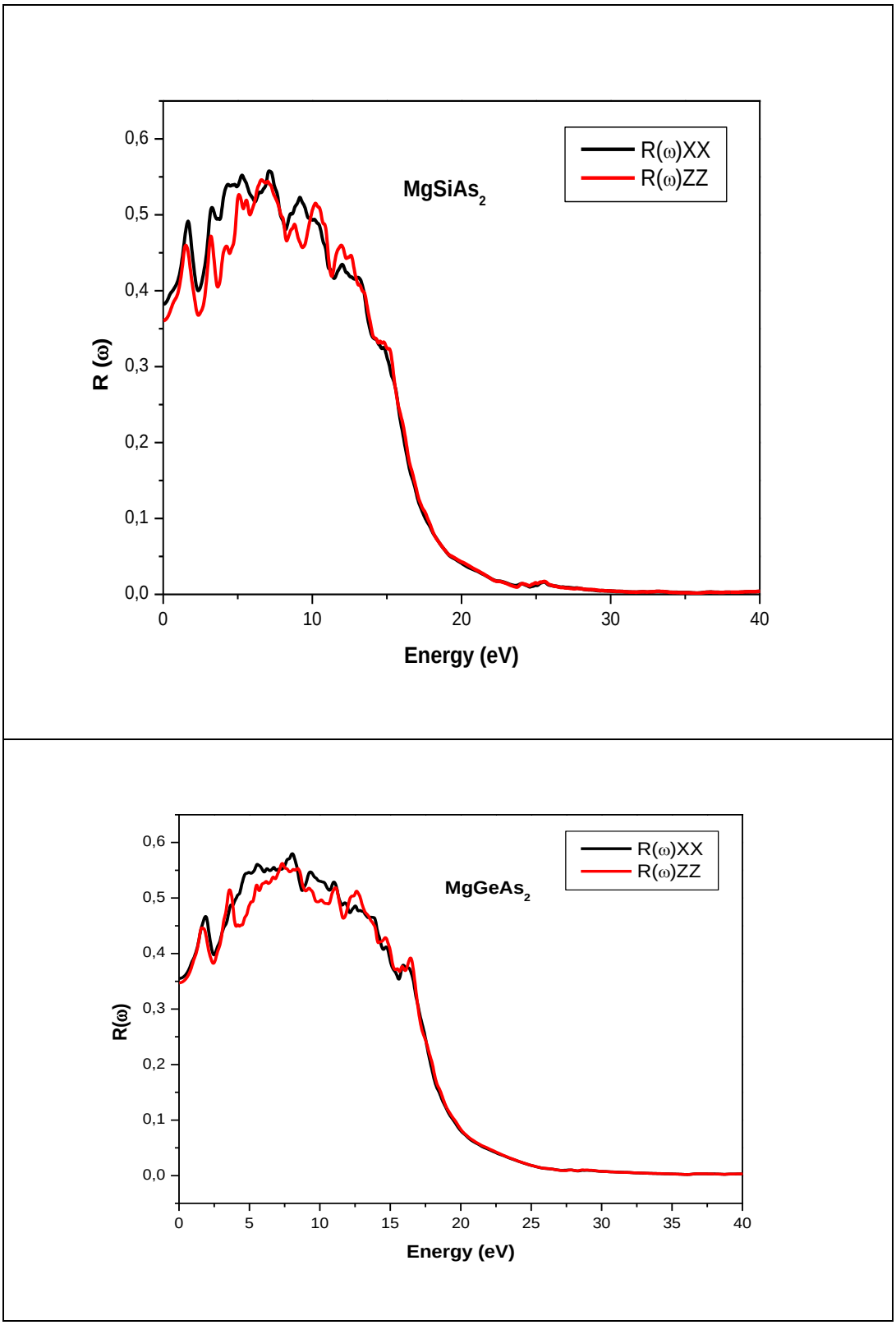

Figure IV-6: Variation of optical reflectivity R (ω) as a function of photon energy for MgGeAs2 and MgSiAs2compounds.

E- Absorption

The variation of the absorption coefficient as a function of energy is shown in figure (IV-7) for MgGeAs2 and MgSiAs2. We can note that the fundamental absorption thresholds start at around 0.30, 0.09 eV for CuInSe2 and CuInTe2, respectively. The curves show a maximum at energies 9.89 and 6.56 eV for the compounds MgGeAs2 and MgSiAs2 respectively.

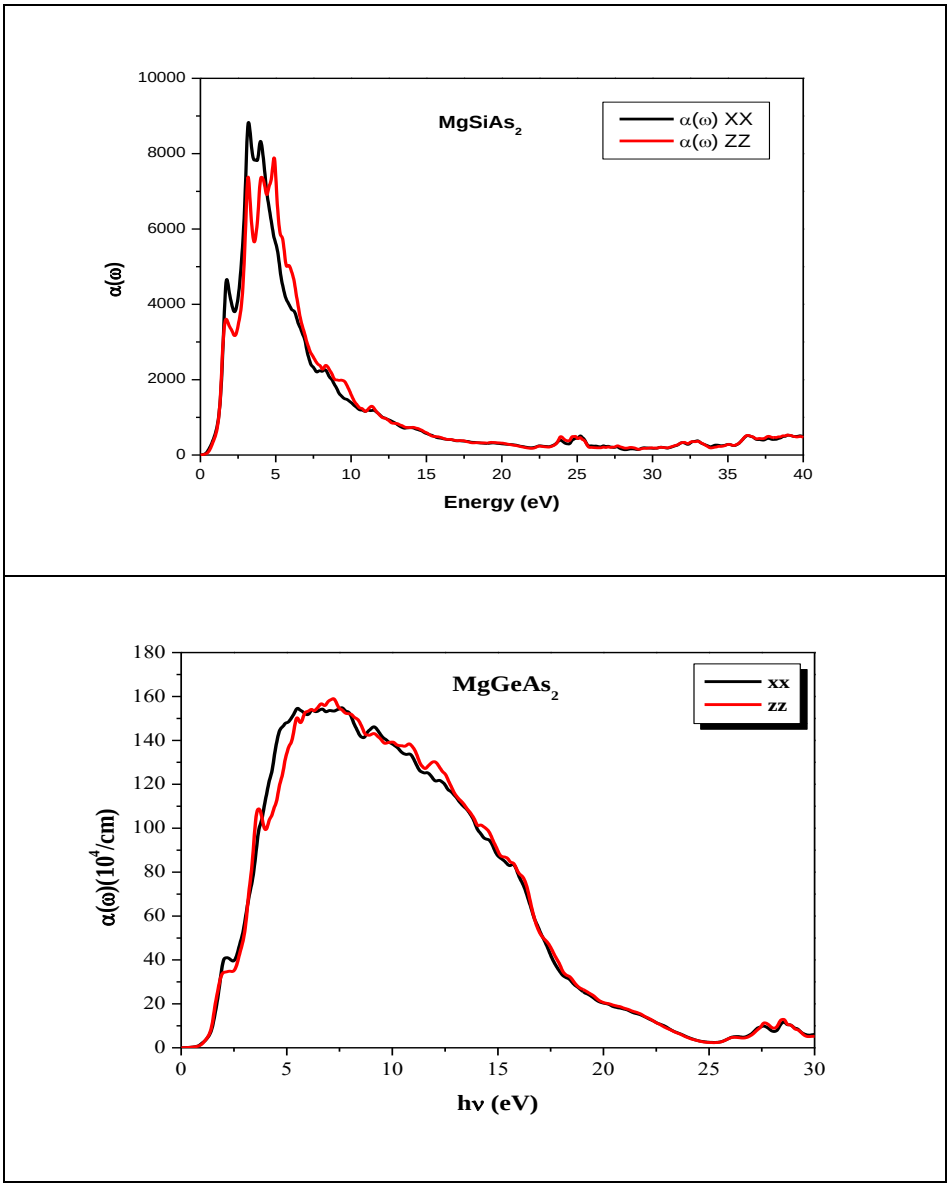

Figure IV-7: Variation of the absorption coefficient as a function of energy for the compounds MgGeAs2 and MgSiAs2.

IV-4. Conclusion

During this work, we studied the structural, electronic and optical properties of MgGeAs2 and MgSiAs2 compounds. The calculations were performed by the ab-initio method called augmented plane waves (FP-LAPW) within the framework of density functional theory (DFT).

- The structural results such as the lattice parameter and the compressibility modulus are in good agreement with the theoretical and experimental values available in the literature.
- The study of the structures of the electronic bands allowed us to conclude that the gap is direct. The calculated values of the gaps of these compounds by using (WC-GGA) and (mBj) correspond well to the theoretical data.
- The most interesting for a semiconductor is the optical properties. We have determined the complex dielectric function and the refractive index. The results obtained are in good agreement with those of other theoretical calculations.

General conclusion

General concluison

In this work, we studied the structural, electronic and optical properties of the ternary compounds Mg(Si, Ge)As2. The calculations were performed by the Linearized Augmented Plane Wave (FP-LAPW) method as part of the density functional (DFT) implemented in code (Wien2K). To determine the exchange and correlation potential, we used the local density approximation (LDA) and the approximation (LDA-mBJ).

• The mesh parameters (a, c/a) and the internal parameter (u) are in good agreement with the theoretical results and the experimental data.

• The compressibility modulus $B0$ and its derivative $B0'$ of Mg(Si, Ge)As2 are in agreement with the theoretical results and the experimental data.

• The band structures calculated for these compounds indicate the presence of a direct gap at the Γ high symmetry point of 1.875 eV and 1.826 eV for the two materials MgSiAS2 and MgGeAs2 respectively, by exploiting the (mBJ) approach. The results

calculated are in agreement with other theoretical calculations and are underestimated compared to experimental data.

• The curves of the densities of states are similar for the approximation (mBJ) with a slight difference. The total and partial state densities of the chalcopyrite phase show that the valence bands mainly consist of all s/p - states (Mg, Si, Ge and As).

• A good agreement with the experimental was obtained with the mBJ approximation concerning the optical parameters.

• The real and imaginary parts by using the Kramers-Kronig relations, the dielectric function. And the optical quantities (Refractive index, absorption, optical reflectivity and optical conductivity). Are in agreement with the results

theoretical and experimental data.

• These materials have a high absorption coefficient in the visible. What will serve positively for the application in the field of optoelectronics.

References:

[1] E. Becquerel, C.R.Hebd. Seances Acd. Sci. 9, 561(1839).

[2] W.Smith, Nature (London) 7, 303 (1873).

[3] W.G Adams and R.E. Day, Proc. R. Soc. London, Ser.A 25, 113(1877).

[4]D.M. Chapin, C.S. Foller and G.L. Pearson, J.Appl. Phys. 25, 676 (1945).

[5] M.A.Arsene, A. Albacete, F.Viollot, J.P. Peyrade, A.Berra, J. Galibert, S.M.Wasim and E.Hernandez, J.Grys.Growth 158, 97 (1996).

[6] J.H.Scofield,A.Duda,D.Albin, B.L.Ballard, P.K.Predecki,thin Solid Films.260,26 (1995).

[7] K.Orgassa.H.W.Shock,J.H.Werner, thin solis Films. 431-432,387 (2003).

[8] L.Assmann, J.C.Bernede, A. Drici, C.Amory, E. Halgand, and M. Morsli, «Study of the Mo thin films and Mo/CIGS interface properties» Applied surface Science, Vol. 246, no.1-3,PP.159-166 (2005).

[9] M.Powalla and B.Dimmler, «Scaling up issues of CIGS Solar Cells»Thim Solid Films, Vol. 361-362, PP. 540-546,Février (2000).

[10] M.A. Contreras, B. Egaas, K. Ramanathan, J. Hiltner, A. Swartzlander, F. Hasoon and R. Noufi, Progress in Potovoltaics: Research and Applications, vol 7, 311 (1999).

[11] A. Luque, Practical Handbook of photovoltaics (Second Edition) (2012).

[12] F.Abdo,thèse de doctorat, institut des nanotechnologies de lyon (INL) à l'INSA de lyon ,France (2007).

[13] A. Bouraiou , thèse de doctorat, Université Mentouri –Constantine (2009).

[14] L. Saad Hamideche, thèse de doctorat, Université badji Mokhtar Annaba (2012).

[15] Benzaghou H. Mostefa Kara S, "Matériaux chalcopyrites élaboration, application photovoltaïque et classification" , Mémoire de DES ,université de Tlemcen (2009).

[16] David L. Jones, .'' The Leaching of Chalcopyrite'', Thèse de doctorat, University of British Colombia, Vancouver 8, Canada(1974).

[17] Jaffe, J. and A. Zunger. "Electronic structure of the ternary pnictide semiconductors ZnSiP2, ZnGeP2, ZnSnP2, ZnSiAs2, and MgSiP2." Physical Review B 30(2): 741 (1984)

[18] Otfried, M. Semiconductors: data handbook, Springer-Verlag(2004).

[19] V.Fock, Z.phys.61, 126, 62, 795 (12927), (1930).

[20] Slater, J.CRev.35,210.(1930).

[21] J.M.Drolot, J.P.Bailon, J.Masounave, des matériaux, édition de l'ecole polytechnique de Montréal.

[22] D.R. Hartree, Proc. Combridge Philos. Soc. 24, 89 (1928).

[23] V. Fock, Z. Phys. 61, 126(1930) ; 62, 795 (1930).

[22]. J.C. Slater, Phys. Rev. 81, 385 (1951).

[25] L.H.Thomas,Pro. Combridge Philos. Soc. 23,542 (1927).

[26]. P.E Lippens, Matériaux complexes, Montepellier (1999).

[27] E. Fermi, Z. Phys., 48, 73(1928).

[28] P.A.M. Dirac, « Note on exchange phenomena in the Thomas-Fermi atom », Proc. Cambridge Phil. Roy. Soc., vol. 26, 1930, p. 376-385.

[29] C.F. von Weizsacker, « Zur Theorie der Kernmassen », Z. Phys., vol. 96,, p. 431 (1935)

[30]. M.L. Doublet, Gallerne 99 : Structure électronique des solides, piriac sur Mer (1999).

[31] P. A. M. Dirac, "Note on exchange phenomena in the Thomas -Fermi atom" Proc.Cambridge Phil. Roy.Soc. 26: 376-385 (1930).

[32] P. Hohenberg, W. Kohn: Phys. Rev. B 864, (1964).

[33] W. Kohn, L. Sham, Phys. Rev., A1133,140 (1965).

[34] T. Starkloff and J.D.joannopoulos, Phys.Rev. B16, 5212 (1977).

[35] G. Kresse, J. Hafner and R.J Needs, J. Phys. Condens. Matter 4, 7451 (1992).

[36] J. P. Perdew, S. Burke et M. Ernzerhof, Phys. Lett. 77, 3865 (1996)

[37] J.P. Perdew, J.A. Chevary, S.H. Vosko, K.A. Jackson, M.R.Pederson, D. J. Singh, and C.

Fiolhais, Phys.Rev. B 46, 6671 (1992).

[38] J.P.Perdew, S. Burke and M. Ernzerhof, Phys.Rev.Lett. 77, 3865 (1996).

[39] S. Kurth,J.P. Perdew. P.Bladha, Int, Quant. Chem. , 75, 889 (1999).

[40] C. Adamo.M.Ernzerhof, G,E. Scusceria, J Chem. Phys, 112,2643 (2000).

[41] B. Hammer, K.W. Jacodeson. J.K. Norskov, Phys. Rev. Lett. 70, 3971 (1993).

[42] C.G. Morgan, P. Kratzer, M. Scheffler. Phys. Lett.82. 4886 (1999).

[43] V. Ozolins. M. Korling. Phys. Rev. B48, 18304 (1993).

[44] F. Bloch, Z. Phys. 52, 555 (1928).
[45] J.C. Slater, « Quantum Theory of Molecules and Solids », V2, Ch. 8 (1965).
[46] C. Herring, Phys. Rev. 57, 1169 (1940).
[47] J.C. Slater, Phys. Rev. 51, 846 (1937).
[48] J. Korringa, Physica 13, 392 (1947).
[49] F.S. Ham, B. Segall, Phys. Rev. 124, 1786 (1961).
[50] O.K. Andersen, Phys. Rev. B 12, 3060 (1975).
[51] J.P. Perdew, Y. Wang, Phys.Rev. B 33, 8800 (1986).
[52] J. P. Perdew in 'Electronic Structure of Solids', Academie Verlag, Berlin, 11(1991).
[53] V. Heine and M. J. G. Lee. Phys. Rev. Lett 27, 811 (1970).
[54] T. Starkloff and J. D. Joannopoulos, Phys. Rev. B 16, 5212 (1977).
[55] R. Zeller, P. Lang, B. Drittler, and P. H. dederichs, in application of multiple scattering
theory to Materials Science, W. H. butler, P. H. Dederichs, A. gonis, and R. Weaver, MRS Symposia Proccedings No. 253, 357 (Materials research Society, Pittsburgh, (1992).
[56] D.D. Koelling and G.O. Arbman, J. Phys. F 5, 2041 (1975).
[57] O.K. Andersen, Phys. Rev. B 12, 3060 (1975).
[58] N. Troullier and J. L. Martins, Phys. Rev. B 43, 1993 (1991).
[59] G. Kresse, J. Hafner and R. J. Needs, J. Phys. Condens. Matter 4, 7451 (1992).
[60] O. K. Andersen, Phys. Rev. B12 3060-3083 (1975)
[61] D. J. Singh, Phys. Rev. B 44, 7451 (1991).
[62] S. Goedecker and K. Maschke, Phys. Rev. B 42, 8858 (1990).
[63] D. J. Singh and H. Krakauer, Phys. Rev. B 43, 1441 (1991).
[64] D. J. Singh, K Schwarz and P. Blaha, Phys. Rev. B 46, 5849 (1992).
[65] L.J.Sham, W.Kohn, Phys.Rev 145 561 (1966).
[66] J. P. Perdew, J. A. Chevory, S. H. Vosko, K. A. Jackson, M. A. Perderson, D. J. Singhand C. Fiolhais, phys Rev. B.46 6671 (1992).

[67] J. P. Perdew, S. Burke and M. Ernzerhof, Phys. Rev.Let.77,3865 (1996).

[68] S. Cottenier, Density Functional Theory and the family of (L) APW-methods: a step-by-step introduction BelguimAugust 6, (2004).

[69] O. K. Andersen, Phys. Rev. B12 3060-3083 (1975).

[70] E. Sjösted, L. Nordström and D. J. Singh, Solid State Commun. 114, 15(2000).

[28] G.H.K. Madsen, P. Blaha, K. Schwarz, E. Sjösted and L. Nordström, Phys. Rev. B. 64,195134(2001).

[71] D. R Hamann, Phys. Rev. Lett. 212, 662 (1979).

[72] P. Blaha, K. Schwarz, G.K.H. Madsen, D. Kvasnicka and J. Luitz, WIEN2k, An Augmented Plane Wave Plus Local Orbitals Program for calculating Crystal Properties, Vienna University of Technology, Vienna, Austria (2008).

[73] W. A. Harrison, Phys. Rev. B 10, 767 (1974).

[74] W. A. Harrison and S.Ciraci, Phys. Rev. B 10, 1516 (1974).

[75] S. P .Kowaslczyk, L. Ley, F. R. Mc Feely and D. A. Shirley, J. Chem 61, 2850 (1974).

[76] D. R. Penn, Phys. Rev. 128, 2093 (1962).

[77] P. J. Stiles, Sol. Stat. Com. 11, 1063 (1972).

[78] D. Shifert, Phys. Rev. B 10, 3316 (1974).

[79] O. K. Andersen, Phys. Rev. B 12, 3060 (1975).

[80] P. Blaha, K. Schwarz, G. K. H. Madsen, D. Kvasnicka and J. Luitz, WIEN2K: An Augmented Plane Wave Plus Local Orbitals Program for calculating Crystal properties (Vienna University of Technology, Austria, (2008).

[81] P. Hohenberg, W. Kohn, Phys. Rev. B 136, 864 (1964).

[82] W. Kohn, L.J. Sham, Phys. Rev. 140, 1133 (1965).

[83] Z. Wu, R. E. Cohen, Phys. Rev. B 73, 235116 (2006).

[84] F.Tran, P. Blaha, Phys Rev Lett. 102, 226401 (2009).

[85] . F.D. Murnaghan, Proc. Natl.Acad. Sci. USA 30 -5390 (1944).

[86] N. G. Dhere, M. C. Lourenço and R. G. Dhere, Solar Cells. 16, 369-380 (1986).

[87] Fiche JCPDS No 80-2189 (2001).

[88] D. Suri, K. Chapdal and G. Chadha, J. Appl. Cryst. 22, 578 (1989).

[89] J. P. Perdew, K. Burke and M. Ernzerhof, Phys. Rev. Lett. 77, 3865 (1996).

[90] C. Domain, S. Laribi, S. Taunier, J. F. Guillemoles, J. Phys. Chem. Solids. 64, 1657 (2003).

[92] R. R. Philip and B. Pradeep, Thin Solid Films. 472, , 136 (2004) .

[93] G. Marin, S.M. Wasim, G. Sanchez Pérez, B. Bocaranda and E. Mora, Journal of Electronic Materials. 27, , 1351 (1998) .

[94] B. A. Mansour, S. A. ABD-EL-Hady, A. ABD-EL-Alli, I. K. EL-Zawawi, Fizika A 12 275 (2003).

[95] V.Fock, Z.phys.61, 126, 62, 795 (12927), (1930).

[96] C. Ambrosch-Draxl, J. O. Sofo, Comput. Phys. Commun. 175, (2006) 1.

[97] N. M. Ravindra, S. Auluck, V. K. Srivastava, Phys. Status Solidi B 93- K155(1979).

[98] R. R. Reddy, Y. Nazeer Ahammed, K. Rama Gopal, D.V. Raghuram, Opt. Mater.10-98(1998).

[99] R.M. Wentzcovitch, M.L. Cohen, P.K. Lam, Phys. Rev. B 36 -6058(1987).

[100]A . Shankar1*, R. K. Thapa2 and P. K. Mandal1, Journal of Physics: Conference Series 765 -012008(2016).